OBLIQUE ELECTROMAGNETIC REFLECTION FROM LAYERED LUNAR MODELS

Technical Report
NASA Contract NAS 2-5078

Final Progress Report for
Item 311A, NASA Contract NAS 2-5078
for submittal to the National Aeronautics
and Space Administration

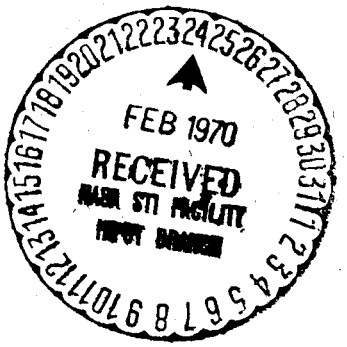

Space Sciences Laboratory
Series 11, Issue 7

UNIVERSITY OF CALIFORNIA, BERKELEY

OBLIQUE ELECTROMAGNETIC REFLECTION FROM LAYERED LUNAR MODELS

By

G. R. Jiracek

and

S. H. Ward

Technical Report on NASA Contract NAS 2-5078 (Item 311A)

January 1970

ABSTRACT

Specular reflection of an arbitraily polarized plane wave incident upon lunar models consisting of discrete plane layers is completely determined by two orthogonal complex reflection coefficients. These measurable quantities together with derived values of apparent conductivity and dielectric constant as functions of frequency and/or angle of incidence are diagnostic of the electrical properties and vertical extents of the various discrete and homogeneous layers. Inference as to the presence of water at depth is thereby facilitated. Computations in the frequency range 10^4 to 10^{10} Hz emphasize the desire for continuous frequency or incident angle sampling over wide ranges to reduce interpretational ambiguities caused by aliasing. The substitution of a gradational debris layer for a homogeneous one does not alter the above conclusions, but at high frequencies the results reflect the properties only of the very top of the gradational debris. Reflection from layers having magnetic permeabilities other than free space is investigated and it is concluded that the measurement of orthogonal polarizations may in practice identify this condition. If existing magnetic permeability is not accounted for, dielectric constant values significantly lower than actual may be interpreted. Bistatic-radar results presented at 136.11 MHz clearly show that large changes in reflectivity may be the result of very small changes in debris thickness. In practice, an orbital sounding is an average over a considerable areal extent, thus interpretations based on laterally homogeneous layering are generally shown to require some modification.

OBLIQUE ELECTROMAGNETIC REFLECTION FROM LAYERED LUNAR MODELS*

1. Introduction

The specific problem which we wish to analyze is the determination of the scattered field returned from the moon when illuminated by plane electromagnetic waves. We shall consider the lunar interior as radially layered in some sense. To estimate the electromagnetic properties of these layers we shall use our current knowledge of earth materials (admittedly inadequate) and the available data obtained from lunar studies. In addition to the layering assumption, we shall further approximate the situation by neglecting several factors. Lateral inhomogeneities and anisotropy are omitted in the layers as is any distribution of objects immersed in these layers. Our model of the moon shall consist of a plane surface and parallel plane interfaces between layers. Thus, the gross spherical layering of the moon is assumed planar; this is permissible when the radius of curvature for the various layers is much greater than the electromagnetic wavelength in the media. By assuming no discrete scattering centers within layers and foregoing surface and interface roughness we necessarily disregard multiple scattering and shadowing involving these sources. We have derived results in the frequency range 10^4 to 10^{10} Hz which seems a practical frequency band for the orbital studies of immediate concern. Free space is assumed above the lunar surface although anomalous propagation is expected in the vicinity of the estimated electron plasma frequency of 2.8×10^4 Hz in the solar wind (Phillips, 1968). On the anti-solar side of the moon, plasma resonances are expected to be well outside the passband of interest in this study. Results are obtained at various

* This work supported by NASA Contract NAS 2-5078.

angles of incidence so that both astatic and bistatic sounding is treated. Incident electric field polarizations both in and perpendicular to the plane of incidence ($E_{\parallel}^{I}$ and $E_{\perp}^{I}$ respectively) have been considered.

From a practical point of view it would seem that our neglect of roughness could be the most serious omission, especially at the higher frequencies. Roughness, though defined arbitrarily, is a function not only of the surface parameters such as slopes and heights but also of the incident radiation, e.g. its wave length and angle of incidence. It is also well known that surface roughness can modify the returned signal much more than the electrical properties of the half space (Beckmann and Spizzichino, 1963). This modification reduces the specular component in reflection and introduces an incoherent signal composed of components differing randomly in phase and amplitude from the specular return.

2. Theoretical Approach

a. Arbitrary Polarization

The scattered return or modification of the radiation incident upon a planetary surface may be described by a number of schemes. We could characterize the illumination and scattered fields by their four Stokes parameters in which case the Mueller matrix describes the transformation (Hagfors, 1967). Alternatively, the transmitted electric field can be thought of as being transformed to the scattered return by the composite target scattering matrix (Huynen, 1967). Obtaining this matrix directly requires measuring amplitude and phase of two orthogonal returns from each of two transmitted orthogonal signals. Other indirect methods

necessitate amplitude (or power) measurements only. Huynen (1967) has shown that the formulation of a composite scattering matrix to characterize backscattering by rough surfaces may be used to represent the modified Kirchhoff-Huygens approach presented by Fung (1966). Our model of the lunar surface treats specular refection only; therefore, a single rather than a composite scattering matrix will be used to describe the returned signal.

Suppressing range and time dependence terms the scattering matrix in our application becomes simply the 2 x 2 matrix in

$$\begin{bmatrix} E_{\parallel}^{S} \\ E_{\perp}^{S} \end{bmatrix} = \begin{bmatrix} R_{\parallel} & 0 \\ 0 & R_{\perp} \end{bmatrix} \begin{bmatrix} E_{\parallel}^{I} \\ E_{\perp}^{I} \end{bmatrix} \tag{1}$$

where the superscripts I and S refer to the incident and scattered electric fields for the two polarizations. $R_{\parallel}$ and $R_{\perp}$ are the complex orthogonal electric field reflection coefficients for the layered half-space. From (1) it is apparent that, except when the incident field is solely $E_{\parallel}^{I}$ or $E_{\perp}^{I}$, depolarization, that is, a change in polarization, results even from specular reflection. Thus, though (1) is simple it is far from trivial.

The notation in (1) easily accomodates arbitrary incident polarization when we write the components of incident $\vec{E}^{I}$ as

$$E_{\parallel}^{I} = \left|E_{\parallel}^{I}\right| e^{i\phi_{\parallel}^{I}}$$

$$E_{\perp}^{I} = \left|E_{\perp}^{I}\right| e^{i\phi_{\perp}^{I}} \tag{2}$$

The relative phase $\phi = (\phi_{\parallel}^{I} - \phi_{\perp}^{I})$ of the incident components describes the sense and degree of elliptical polarization which degenerates to linear when ϕ equals $0, \pi, 2\pi, \ldots$ Figure 1 gives the usual geometrical representation of the locus of the electric field vector in a plane normal to the incident direction. The angle between the major axis of the ellipse and the normal to the incident plane is the orientation angle ψ whereas τ $(-\pi/4 < \tau \leq \pi/4)$ is refered to as the auxiliary or ellipticity angle. The sign of τ differentiates left-handed (-) from right-handed (+) polarization. Following Huynen (1967), we express $\vec{E}^{I}$ as

$$\vec{E}^{I} = \begin{bmatrix} E_{\parallel}^{I} \\ E_{\perp}^{I} \end{bmatrix} = |\vec{E}^{I}| \begin{bmatrix} \sin\psi & \cos\psi \\ \cos\psi & -\sin\psi \end{bmatrix} \begin{bmatrix} \cos\tau \\ i\sin\tau \end{bmatrix} \qquad (3)$$

This combined with (1) describes the scattered field conveniently in terms of the polarization geometry of the incident field. Such a resolution of the incident polarization is necessary in practice for the ultimate decomposition of (1) to yield orthogonal reflection coefficient values.

It has been previously shown by Ward, Jiracek and Linlor (1968) that estimates of the electrical properties of hypothesized lunar layers may be obtained from values of the reflection coefficients at normal incidence. The present study further generalizes the results to oblique angles of incidence; thereby, permitting bistatic analysis of differing incident polarization states. Figure 2 diagramatically represents a plane wave obliquely incident upon a layered lunar structure at an angle θ. Each layer of thickness h_j is assigned dispersive values of permittivity ϵ_j, conductivity σ_j, and magnetic permeability μ_j.

Theoretical evaluation of the reflection coefficients for the two polarizations follows Wait (1958).

b. Parallel Polarization

The amplitude reflection coefficient for this case is obtained from

$$R_{11} = \left|R_{11}\right| e^{i\phi_{R_{11}}} = \frac{Z_a - Z_o}{Z_a + Z_o} \tag{4}$$

In (4) the surface impedance Z_a is found by the recursive relation

$$\begin{aligned} Z_a &= Z_1 \frac{\hat{Z}_2 + Z_1 \tanh(u_1 h_1)}{Z_1 + \hat{Z}_2 \tanh(u_1 h_1)} \\ \hat{Z}_2 &= Z_2 \frac{\hat{Z}_3 + Z_2 \tanh(u_2 h_2)}{Z_2 + \hat{Z}_3 \tanh(u_2 h_2)} \\ &\vdots \\ \hat{Z}_{n-1} &= Z_{n-1} \frac{\hat{Z}_n + Z_{n-1} \tanh(u_{n-1} h_{n-1})}{Z_{n-1} + \hat{Z}_n \tanh(u_{n-1} h_{n-1})} \end{aligned} \tag{5}$$

where

$$Z_j = \frac{u_j}{\sigma_j + i\omega\epsilon_j} \qquad j = 0, 1, 2, \cdots, n \tag{6}$$

is the characteristic impedance of the jth layer and

$$u_j = \left(\lambda^2 + \gamma_j^2\right)^{1/2} \tag{7}$$

Here ω is, as usual, the angular frequency, $2\pi f$. The propagation "constant" for each layer is

$$\gamma_j^2 = i\omega\mu_j\left(\sigma_j + i\omega\epsilon_j\right) \tag{8}$$

and

$$i\lambda = \gamma_o \sin\theta \tag{9}$$

The nth layer is semi-infinite; therefore $\hat{Z}_n = Z_n$. By considering Z_a as being equal to the impedance of an equivalent homogeneous half-space we use (6), (7), and (8) to obtain

$$\sigma_a + i\omega\epsilon_a = \frac{i\omega\mu_a \pm \left[(-i\omega\mu_a)^2 + 4Z_a^2\lambda^2\right]^{1/2}}{2Z_a^2} \tag{10}$$

where the a subscript on σ , ϵ , and μ denote apparent values. A + or - sign in (10) is used depending on whether the phase of Z_a is greater than or less than 0° respectively.

c. Perpendicular Polarization

The solution of the reflection coefficient with this polarization is

$$R_\perp = |R_\perp| e^{i\Phi_{R\perp}} = \frac{Y_o - Y_a}{Y_o + Y_a} \tag{11}$$

where the surface admittance Y_a is given by a recursive relation equalling (5) when Z's are replaced by Y's . In this case

$$Y_j = \frac{u_j}{i\mu_j \omega} \qquad j = 0, 1, 2, \cdots, n \qquad (12)$$

are the characteristic admittances of the layers. Using the surface admittance, from (7), (8), and (12) we compute apparent σ , ϵ , and μ using

$$\sigma_a + i\omega\epsilon_a = \frac{(i\omega\mu_a Y_a)^2 - \lambda^2}{i\omega\mu_a} \qquad (13)$$

In practice, after the decomposition of the scattered fields using (1) and (3) to obtain $R_{\parallel}$ and $R_{\perp}$ we would calculate the apparent conductivity and apparent dielectric constant $K_a = \epsilon_a/\epsilon_o$ using (10) and (13) by assuming $\mu_a = \mu_o$. This may not be the actual case, in fact the μ_j's (hence μ_a) may be complex which will be considered briefly in a latter section. Actually, the calculation of apparent electrical quantities is only an interpretational aid. The amplitudes and phases of $R_{\parallel}$ and $R_{\perp}$ do in themselves contain all of the available information relating to layering, depth extent, and electromagnetic properties. To study the behavior of $R_{\parallel}$ and $R_{\perp}$ (also σ_a and K_a) we note that these quantities are functions of both f and θ. For presentation, we shall, therefore, fix one of these parameters while showing the dependency upon the other.

3. Selection of Lunar Models

Detailed discussions of the estimates of the distribution of electromagnetic parameters in the moon may be found in Ward, Jiracek, and Linlor (1968, 1969) and Ward (1969). Herein we shall represent the lunar interior by the following layers: debris, "dry" rock, permafrost, a wet shell, and a hot interior. Except in a later section where the debris is described as a gradual transition, all layers are considered homogeneous. Figures 3, 4, and 5 give estimates of the conductivity, dielectric constant, and loss tangent (tan $\delta_j = \sigma_j/\omega\epsilon_j$) for each layer as functions of frequency in the range 1 to 10^{10} Hz. The near-surface dielectric constant and conductivity values adopted in the radar frequency range are consistent with the most recently reported astatic and bistatic radar results (Burns, 1969 and Tyler, 1968). The full curves represent approximations derived from these and the other references cited above when simple analytic expressions are desirable. Note that each parameter plots as a power function of frequency, i.e. linear segments on a log-log basis. Geologically speaking the debris parameters approximate those of an oven dried volcanic ash and the dry and wet rock layers are consistent with oven dried basalt and basalt with about 1% pore moisture, respectively. The permafrost curves are near to those expected for a rock with a few percent frozen moisture at about -20 to -30 °C. In the frequency range we consider, we do not "see" the posulated hot interior where temperatures in excess of 1500 °C are expected.

4. Results

a. Preliminary Remarks

Our study of oblique electromagnetic reflection from layered models essentially reduces to the interpretation of the complex reflection coefficients in (4) and (11). With layered media it is evident that reflections from subsurface layers will interfere with the surface reflection. This phenomena results in oscillatory behavior in the amplitude and phase of the reflection coefficients as functions of frequency as demonstrated by Ward, Jiracek, and Linlor (1968) for normal incidence. Similar character is found as a function of incident angle and for illustration we shall consider a model consisting of free space overlying a thin layer (first layer) of debris, which in turn overlies a homogeneous half space (second layer). For simplification we treat the strata as nonmagnetic and lossless. The latter condition is expected for lunar near-surface materials where $\tan \delta << 1$ (Figure 5) but magnetic permeability may differ from free space as discussed later. It is well-known from interference optics that the phase difference between surface reflection and reflection from the first-second layer interface is given by

$$\Delta = \frac{4\pi h_1}{c} f \sqrt{K_1} \left(1 - \frac{\sin^2\theta}{K_1}\right)^{1/2} \qquad (14)$$

where c is the velocity of electromagnetic radiation in free space, and $K_1 = \epsilon_1/\epsilon_0$ and h_1 are the dielectric constant and thickness of layer

1 respectively. We expect increasing admittances with depth in the moon; therefore, in the lossless, nonmagnetic case, the surface and primary interface reflections are in phase for perpendicular polarization. Hence, when

$$\sin\theta = \left[K_1 - \frac{c^2}{f^2}\,\frac{(2\ell+1)^2}{16\,h_1^2}\right]^{1/2} \qquad \ell = 0,1,2,\ldots \qquad (15)$$

there will occur interference minima in the $|R_\perp|$ values. This equation also applies to parallel polarization providing the reflections occur at incident angles less than that of the principle or Brewster angle of incidence. At this angle, a phase shift of π occurs in reflection with this polarization and (15) then describes maxima in $|R_{\parallel}|$. Application of (15) to estimate layer thickness h_1 normally requires observation of successive maxima or minima to resolve the interference order ambiquity ℓ. The Brewster angle for surface reflection is obtained from

$$\theta_B = \tan^{-1}\sqrt{K_1} \qquad (16)$$

under the lossless, nonmagnetic assumption when surface reflection vanishes for parallel polarized incident radiation. The Brewster angle at the first layer - second layer interface generally differs from that at the surface. However, for the layers we have postulated, reflection cannot occur at this angle within the moon even with grazing incidence ($\theta = 90°$) upon the surface. In passing, we note that when the layers are not low-loss, the Brewster angle phenomenon does not yield zero reflection

although a minimm occurs at an angle differing from θ_B in (16). Also, if the relative magnetic permeability of a lossless surface layer is greater than the dielectric constant, zero reflection occurs at a specified incident angle for perpendicular polarization. Neither of these environments is expected in the lunar surface except as rare occurences.

To analyze the character of the phase component in reflection we solve (4) and (11) obtaining

$$\phi_{R_{11}} = \tan^{-1}\left(\frac{-2 Z_o |Z_a| \sin \phi_{Z_a}}{|Z_a|^2 - Z_o^2}\right)$$

and (17)

$$\phi_{R_\perp} = \tan^{-1}\left(\frac{-2 Y_o |Y_a| \sin \phi_{Y_a}}{Y_o^2 - |Y_a|^2}\right)$$

Further, we constrain the phase values to be $-\pi/2 < \phi_{R_{11}}, \phi_{R_\perp} \leq \pi/2$. With this constraint and from (17) it is apparent that the phase of the reflection coefficients will pass through 0° discontinuously when $|Y_a| = \pm Y_o$ or $|Z_a| = \pm Z_o$. Continuous oscillations in phase passing through 0° occur when $2 Z_o |Z_a| \sin \phi_{Z_a}$ or $2 Y_o |Y_a| \sin \phi_{Y_a} = 0$.

For a homogeneous half space, with no unusual magnetic properties $Y_o < |Y_a|$ and no discontinuous phase changes occur in $\phi_{R_\perp}$. In

the case of parallel polarization $\mathcal{Z}_o > |\mathcal{Z}_a|$ at less than the Brewster angle of incidence and $\mathcal{Z}_o < |\mathcal{Z}_a|$ above this angle. Therefore, for homogeneous ground a phase change of π is found at the Brewster angle in this case. The numerators in the arguments in (17) dictate 0° phase terms when $\mathcal{Z}_o$ (or $\mathcal{Y}_o$) or the imaginary part of $\mathcal{Z}_a$ (or $\mathcal{Y}_a$) equals zero. $\mathcal{Z}_o$ (or $\mathcal{Y}_o$) is zero only at $\theta = 90°$ as is evident from (6), (7), and (9). The imaginary part of $\mathcal{Z}_a$(or $\mathcal{Y}_a$) is zero for homogeneous ground only when $\tan \delta = 0$, i.e. for pure dielectric materials.

Reflection from a stratified medium is much more complicated than the homogeneous case. During oscillatory behavior in reflection coefficients discontinuities in phase appear whenever the poles in (17) occur. Maxima and mimina in the amplitudes of the reflection coefficients are accompanied by zeros in the phase terms when the materials are low-loss. Physically, the internal reflections return to the surface alternately in-phase and out-of-phase with the surface reflection and the sine terms in (17) yield zeros in the phase response.

All numerical results presented within are obtained by discrete frequency or incidence angle sampling of the appropriate equations. In some cases this sampling rate has been purposely reduced to illustrate the effects of aliasing.

b. Functions of Frequency

For the first lunar model we consider the simple two-layered "dry" moon diagrammed in Figures 6 and 7. Here 10 meters of "dry" debris covers

a crust of solid "dry" rock. Figures 6 and 7 illustrate the amplitude and phase, respectively, of the reflection coefficient as functions of frequency at normal incidence. At vertical incidence the distinction between parallel and perpendicular polarization vanishes hence (4) and (11) yield equal results. The oscillations in these plots are due to the 10 m debris layer and an observation of the first minimum in $|R|$ at 4 MHz would enable the estimate of this thickness to be made. The procedure in practice is discussed by Ward, Jiracek, and Linlor (1968, 1969) and we briefly illustrate the method. To permit using (15) we require an estimate of K_1. Equations (11) or (13) could be invoked but for simply obtaining the layer thickness we note that the low values of reflection coefficient can only arise from low-loss materials. Hence, K_1 may be estimated without phase information in the frequency vicinity of the first minimum by

$$|R| = \left| \frac{1 - \sqrt{K_a}}{1 + \sqrt{K_a}} \right| \tag{18}$$

The mean of $|R|$ is estimated to be 0.27 at 4 MHz and by (18) $K_1 \simeq 3$. Substitution into (15) then yields the layer thickness of 10 m. At low frequencies, only the second layer is influential and (18) yields $K_2 = 7.7$ as opposed to the actual value of 7.8 at 10^4 Hz. Comparison of the oscillations in the phase component (Figure 7) with those of (Figure 6) reveals zeros in ϕ_R at maxima and minima in $|R|$ as expected for low-loss media. Observing low values of reflection coeffecient directly infers low-loss materials and for most natural

substances at temperatures $\gtrsim$ - 40° C this precludes appreciable (a few tenths of a percent) liquid or frozen water. This important determination may therefore require measurements of the amplitude of reflection coefficients only, preferably at low frequencies.

The numerical calculations made to obtain the curves in Figures 6 and 7 (also Figures 8, 11, 12, and 14) utilized 90 equally spaced points to describe the 10^7 to 10^8 frequency decade. These results are generally sufficiently detailed to trace the continuous curves; but, above 10^8 Hz only 9 points per decade are calculated and severe aliasing is present in Figures 6, 7, 8, and 11. Similar aliasing using 30 points per decade is seen in Figures 11 and 12 from 10^6 to 10^7 Hz when these curves are compared to corresponding results in Figures 8 and 14 where 90 points were used. We are thus cautioned that incorrect conclusions may be obtained from discrete observations at too few frequencies.

In contrast to the dry model just considered we now observe the response from the model shown in Figures 8 through 12. Here we have hypothesized a permafrost layer at 100 m depth, extending to 3 Km. A wet shell and hot interior are considered reasonable below this depth but these layers are not influential in the frequency range we have chosen. The major difference between this permafrost model and the dry model occurs at the lower frequencies where the reflection coefficients are higher by about 5 db in the permafrost case. A wet unfrozen layer at 100 m depth would also have reflection coefficients higher than the dry case and in fact could have values as high or higher than the permafrost. The first minimum in $|R|$ at 3×10^5 Hz (Figure 8) is due to the combined thicknesses of the first two layers of 100 m. The oscillations

due to the 100 m thickness damp out as frequency increases and are superimposed upon by another resonant effect with a first minimum at about 4×10^6 Hz. This is due to the 10 m debris layer. Estimation of these depths from actual data requires an estimate of the effective dielectric constant at the various frequencies and this may be done with the aid of Figure 9. This figure graphs the results from the imaginary parts of (10) or (13) and also includes the actual layer values. At high frequencies the oscillations center about and asymptote to the values of the debris layer while at lower frequencies the permafrost values are inferred. Similarly in Figure 10, plotting the real parts of (10) or (13), the conductivities of the debris and permafrost may be estimated from σ_a values at high and low frequencies respectively. It is our experience that values of σ_a asymptote much less rapidly and are less regular than corresponding apparent dielectric constant values. The phase component of R for the permafrost model contains numerous discontinuities in the range of the predominance of the 100 m layer hence is not displayed graphically.

Figures 11 and 12 present results at $\theta = 60°$ with the permafrost model for the two electric polarizations. As the angle of incidence is increased, there is a general increase in the values of $|R_\perp|$ and the oscillations are shifted due to slant path changes as required by (15). With parallel polarization, an overall decrease in the reflection coefficient values together with migrations in the oscillations are observed until reaching the Brewster angle. This angle is a function of frequency since we have inserted dispersive electrical properties for the layers. In Figure 12 we see that above 10^9 Hz the Brewster angle

may be taken as 60°. This is verified by (16) when using $K_a \simeq K_1 = 3$ above 10^9 Hz (Figure 9). The nulls in the reflectivity at Brewster angles can be used directly to estimate dielectric constant as has been done for the moon by Tyler (1968) employing bistatic-radar measurements. The phase change of π as we pass through the Brewster angle results in reversals in the troughs and peaks in $|R_{\parallel}|$ at higher angles of incidence. As the obliquity increases, all $|R_{\parallel}|$ values increase to unity at $\theta = 90°$ as do the $|R_{\perp}|$ values which are not affected by the Brewster angle phenomenon.

The Apollo 11 results (Lunar sample preliminary examination team, 1969) have confirmed a density increase with depth in the lunar surface material as one would expect from simple compaction. To investigate a model of the moon in which debris compaction is accounted for, we have exponentially graded the values of dielectric constant and conductivity from the surface to 10 m depth by considering 100 discrete 0.1 m layers as shown for 136.11 MHz in Figure 13. The gradational values have been adopted as functions of frequency similar to the functions given in Figures 3 and 4. The reflection coefficients presented in Figure 14 at normal incidence result. At low frequencies, this curve is identical to that of Figure 8 which pertains to a homogeneous 10 m surface layer. However, the superimposed oscillations due to the 10 m layer, so well developed in Figure 8, are barely discernible in Figure 14. Also the $|R|$ high frequency asymptote is much lower in the gradational case. At wave lengths substantially less than the thickness of the gradational layer, reflection is most sensitive to the contrast in dielectric constant occurring at the surface. Hence, the reflection

coefficient and associated quantities identify the surface discontinuity above about 5 x 10^7 Hz even though the skin depth is as great as 50 m. The irregularities in $|R|$ at approximately 10^9 Hz and above are due to the 100 discrete layers used to approximate a continuous gradational change. In the limit of an infinite number of layers, the results can be shown to converge (Fuller and Ward, 1969).

c. Functions of Angle of Incidence

To study the effect of a bistatic-radar system illuminating the moon at angles of incidence 0 to 90° we have chosen to present results at 136.11 MHz which is the frequency used in Tyler's experiments. The results for parallel polarization are presented in Figures 15 and 16 and show the dependence on debris thickness using the permafrost model. Many of the features discussed in part (a) of this section may be deduced from these figures. Oscillations in the apparent dielectric constant curves are in phase with $|R_{||}|$ oscillations at frequencies below the Brewster angle and out-of-phase above as close examination of the h_1 = 30 m results of Figure 15 will confirm. The Brewster minima, e.g. at 60° for h_1 = 100 m, are accompanied by discontintuities in the phase of the reflection coefficient as Figure 16 illustrates. Continuous change of phase $\phi_{R_{||}}$ through zero degrees appears at oscillatory maxima and minima in $|R_{||}|$. The phase $\phi_{R_{||}}$ is zero at grazing incidence. Oscillations in apparent conductivity, Figure 16, are nearly out of phase with the $|R_{||}|$ values. These general patterns are expected when tan $\delta \ll 1$ pertains in the materials.

With h_1 = 100 m the amplitude and phase of the reflection coefficients appear as smooth functions of incident angle except at the Brewster angle

of 60° (Figures 15 and 16). The apparent dielectric constant yields, for h_1 = 100 m, a value of 3 for all angles of incidence; this value is also evident using (16) at the Brewster angle. The apparent conductivity does, however, show oscillatory behavior due to the 100 m thickness (Figure 16). In this theoretical case the actual conductivity and thickness of layer 1 can be estimated but in practice, equipment resolution would limit this capability. $|R_{\parallel}|$, $\phi_{R_{\parallel}}$, and K_a curves for the 10 m and 30 m debris layers oscillate about the 100 m results yielding appropriate thickness values via (15). The apparent conductivities, though, are not directly useful in determining σ_1 or σ_2 values. Because 1 m is nearly an exact odd multiple of a quarter wave at the frequency chosen, we have seemingly anomalous results for this debris thickness. Actual definition of all of these curves ultimately depends upon equipment resolution and sampling characteristics.

As an example of using (15) to determine layer thickness we take the successive h_1 = 10 m minima in $|R_{\parallel}|$ at 17° and 42°. Setting K_1 = 3 and substituting 17° and 42° to obtain two simultaneous equations in the two independent unknowns ℓ_{17} and h_1 yields ℓ = 15 and 14, respectively, and $h_1 \simeq 10$ m. (Note that $\ell_{42} = \ell_{17} - 1$ so that ℓ_{42} is not an independent unknown.) It is possible to estimate a value of dielectric constant for layer 2 from peaks of K_a values, e.g. K_2 is likely to be at least as large as 4.5 according to the h_1 = 10 m data of Figure 15.

Figure 17 contains $|R_{\parallel}|$, $|R_{\perp}|$, $K_{a_{\parallel}}$, and $K_{a_{\perp}}$ results for a gradational 10 m debris layer at 136.11 MHz. The reflectivity values plot smoothly with no 10 m oscillations. The occurence of the

Brewster angle at 52° and the values of apparent dielectric constant yield the value of the very top of the debris layer as discussed earlier. The minor irregularities in the K_a plots are the result of the discrete sampling of the continuous debris. It has been found that apparent values calculated from parallel polarization results are more irregular and this is attributed to the Brewster phenomenon. Though not presented graphically, the more sensitive apparent conductivity results contain not only the irregularities due to the 0.1 m layers but also a superimposed 10 m effect. Even if we assume no error in measurements of the incident angle, less than 1 db resolution in $|R|$ would be necessary to resolve such σ_a variations.

We have assumed, above, that magnetic permeability is that of free space in all layers although preliminary measurements on Apollo 11 lunar samples yield values of permeability μ as high as $1.5\,\mu_o$ (Lunar sample preliminary examination team, 1969). Furthermore, measurements, performed at the Massachusetts Institute of Technology Laboratory for Insulation Research, on samples of Hawaiian basalts reveal a frequency dependence of μ and the existence of a loss or imaginary component at high frequencies (Westphal, personal communication). For example, at 300 MHz, real $\mu = 1.17\,\mu_o$ and tan $\delta_m = 0.008$ (tan $\delta_m = |\text{imaginary}\,\mu / \text{real}\,\mu|$). The influence on reflectivity of $\mu \neq \mu_o$ in a homogeneous half space is to decrease $|R|$, K_a, and σ_a values at normal incidence when μ/μ_o is less than ϵ/ϵ_o. For layered models the effect is less clear and to exemplify this, we have chosen real $\mu = 1.25\,\mu_o$ and tan $\delta_m = 10^{-3}$ in the permafrost model at 136.11 MHz. For a debris thickness h_1 of 10 m, the reflection coefficients $|R_{\parallel}|$ and $|R_{\perp}|$ are plotted in Figure 18 where they are compared to the $\mu = \mu_o$ case. Note the reflection decrease due

to $\mu \neq \mu_o$ at normal incidence. To evaluate the apparent electrical properties we assume $\mu = \mu_o$ in (10) and (13) since this would be the case if we had no prior knowledge of the magnetic properties. The results for $K_{a_{||}}$ and $K_{a_{\perp}}$ are presented in the upper portion of Figure 18 where the expected decrease at normal incidence is seen. Dielectric constant values interpreted from astatic reflection results can thus be significantly lower than actual if existing magnetic permeability is not accounted for. A significant difference in the apparent K_a values for the two polarizations due to permeability change occurs at higher angles of incidence. Here we see considerably more divergence in the $K_{a_{||}}$ and $K_{a_{\perp}}$ values than when $\mu = \mu_o$. This may uniquely serve to identify this situation and suggests further investigation pertinent to lunar and terrestial electromagnetic soundings.

In Figure 19, we present idealized bistatic-radar results at 136.11 MHz from a hypothesized lunar profile. In Tyler's experiments the receiver was earth based while the transmitter aboard Explorer 35 orbited the moon. As a consequence, for lunar equatorial orbit, a profile of one quarter of the moon from 0 to 90° longitude plots as 0 to 90° angle of incidence. Each degree of incidence angle in Figure 19 may therefore be thought of as equalling 30 Km of circumferential distance. For this illustration, specular point reflection is assumed and diffraction effects at abrupt vertical boundaries are neglected. No surface debris layer is taken from 0 to 10°. From 10 to 30° the debris thickness is increased to 1 m by 2° steps of 0.1 m each. Other thickness changes are apparent in Figure 19. These variations give rise to the $|R_{||}|$ and $|R_{\perp}|$ signatures as plotted. It is apparent from θ = 10 to 30° that very small changes in thickness can produce very large changes in the reflectivity

values. This is of course the result of the interference between waves reflected from the surface and the debris/rock boundary. The apparent dielectric constant values for the two polarizations follow essentially the same curve since $\mu = \mu_o$. The value of the bed rock ($K_2 = 6$) is evident where it is exposed on the surface (0 to 10°) and the other values vary about the debris value of 3.

In the previous example, we have assumed specular point reflection although in practice the measured reflection properties would represent a response averaged over a region of approximately Fresnel-zone size (Tyler, 1969). For orbital electromagnetic soundings we expect the reflecting region to be as large as tens of kilometers in lateral extent so that debris thickness variations generally would be expected within the area contributing to the return. A rigorous solution to reflection from such a stratified region cannot be obtained from our formulation. However, for a first approximation we shall compute the mean response from a statistical distribution of debris thicknesses. As an example, we regard the debris thickness as equally likely to be a value between 0 and 10 m; that is, the debris exhibits a uniform distribution over this range. The mean reflection coefficients obtained from sampling this distribution at increments of 1 m are plotted in Figure 20 as a function of incident angle. Here we see that the oscillations due to the various thicknesses as illustrated in Figure 15 have been effectively cancelled by the averaging process. Although (15) strictly applies only when reflectivity is zero at the Brewster angle, a dielectric constant of 3 is found using $\theta_B = 60°$ and this is the value of the debris layer. Apparent dielectric constant values determined from (13)

are slightly larger than the input value for the debris as Figure 20 illustrates. Some fluctuations are observed in the K_a values but the vertical scale has been expanded beyond that of typical equipment performance. Most significant, however, is the result that meaningful undulations in the reflectivity curves are not measured even though we have assumed homogeneous layers of discrete thicknesses. This result is of course obtained from a particular distribution of debris depths but it is sufficient evidence to conclude that reflection measurements which reveal no oscillations do not preclude sharply defined debris layers.

Another important consequence of integrating the response from varying debris thicknesses is that the reflectivity at the Brewster angle is not identically equal to zero. Considering low-loss, nonmagnetic materials at the surface leads to reflection coefficient zeros at the Brewster angle only when the surface is homogeneous and thick (h_1 equals 100 m in Figure 15) or when it is gradational as in Figure 17. With the same electromagnetic properties, we observe nonzero Brewster phenomenon either accompanied by reflectivity oscillations (h_1 equals 10 m in Figure 15) or absence of oscillatory behavior (h_1 equals 1 m in Figure 15 and in Figure 20). We therefore conclude that in a low-loss, nonmagnetic, specular reflecting environment, the observation of a Brewster angle minimum significantly different from zero is diagnostic of surface layering of the order of wavelengths in thickness, even if no oscillations are observed in the reflectivity measurements.

5. Discussion and Conclusions

Earth based measurements of the total radar cross section of the moon have been reported (MIT Lincoln Laboratory, 1967) in the 0.008 m

to 22 m wavelength (approximately 1.4×10^7 Hz to 3.7×10^{10} Hz frequency range). There has been a tendency to attribute the apparent increase in cross section with increasing wavelength to systematic errors in the long wavelength results (Evans and Hagfors, 1968). However, more recent results at 6, 7.5, and 12 m (Burns, 1969) strongly support the previous long wavelength results (Davis and Rohlfs, 1964) and reveal a dependence upon the lunar subradar point. A "strong" wavelength dependence in the quasi-specular return near zero time delay (i.e. corresponding to return from the vicinity of the subradar point) has been reported for 0.038, 0.23, and 0.68 m wavelengths (Hagfors, 1967). Early interpretations of the radar cross section results to estimate the lunar surface dielectric constant assumed a homogeneous smooth moon although proof of the contrary is now well established. More recent estimates of the electrical properties of the lunar surface materials have attempted to account for gentle surface undulations Beckmann (1968), scattering from discrete surface and buried sources Hagfors (1967), and a finite thickness of the lunar regolith or debris layer (Hagfors, 1967; Tyler, 1968; and Burns, 1969).

Our results only relate directly to the latter consideration but here several points should be emphasized.

1. We expect electrically low-loss materials in the lunar surface so that reflectivity measurements must be analysed on the assumption that very significant interference effects may occur even at high frequencies.
2. A glance at Figure 8 of our results, for example, shows that reflectivity oscillations can be expected to occur at frequencies as high as 10^9 Hz.

3. The fact that very large changes in reflectivity may be introduced by very small changes in layer thickness must be taken into account.
4. In practice we sample over a considerable area so that the results represent an integrated response from regions in which lateral thickness variations are anticipated. We have demonstrated that such conditions may give rise to a lack of observed reflection oscillations even though sharply defined homogeneous debris layers are present.
5. When considering a debris that is laterally homogeneous but exhibiting electrical properties gradational with depth we found that at wavelengths somewhat less than the thickness of this layer, reflection characteristics are those of the very top of the zone.
6. Measurements at isolated frequencies cannot identify these various effects.

It is tempting to explain the reported wavelength dependence in radar cross section measurements and the related differences in dielectric constants by one or more of the above layering considerations or to magnetic permeability. However, it is our opinion that the dependence of these parameters on non-specular scattering (e.g. due to surface roughness, boulders, etc.) is still insufficiently known to draw such conclusions.

Although we have considered only specular reflection from discrete homogeneous lunar models, the potential merits and problems of orbital electromagnetic soundings have been demonstrated. Our results have

been obtained from the complex reflection coefficients resulting from two orthogonal linear incident polarizations. To help eliminate ambiguities in interpretation we desire both amplitude and phase measurements of these quantities over as large a continuous frequency band as possible. Alternatively, continuous frequency data could be obtained by the spectral decomposition (Fourier transform) of a series of wide band signals, for example, as produced by pulse modulation of a range of carrier frequencies.

References

Beckmann, P., Depolarization of electromagnetic waves backscattered from the lunar surface, J. Geophys. Res., 73, 649, 1968.

Beckmann, P., and A. Spizzichino, The Scattering of Electromagnetic Waves from Rough Surfaces, New York, Macmillan, 1963.

Burns, A. A., On the wavelength dependence of radar echoes from the moon, submitted for publication to J. Geophys. Res., 1969.

Davis, J. R., and D. C. Rohlfs, Lunar radio-reflection properties at decameter wavelengths, J. Geophys. Res., 69 (15), 3257, 1964.

Evans, J. V., and T. Hagfors, Radar studies of the moon, in Radar Astronomy, edited by J. V. Evans and T. Hagfors, pp. 219-273, McGraw-Hill, New York, 1968.

Fuller, B. D., and S. H. Ward, A radially inhomogeneous moon in a plane electromagnetic field, Tech. Rept., Final Rept. Contract NAS2-5242, Space Sciences Lab., Univ. of Calif., Berkeley, 1969.

Fung, A. K., Theory of scattering and depolarization of electromagnetic waves by rough surfaces, Center for Research in Engineering Science, Rept. 48-5, Univ. of Kansas, Lawerence, 1965.

Hagfors, T., A study of the depolarization of lunar radar echoes, Radio Science (new series), 2, 5, 445, 1967.

Huynen, J. R., Radar backscatter from distributed tragets with emphysis on polarization dependence, Lockheed Missiles and Space Co., LMSC-L 86-67-2, Palo Alto, California, 1967.

Lunar sample preliminary examination team, Preliminary examination of lunar samples from Apollo 11, Science, 165, 3899, 1211, 1969.

M.I.T. Lincoln Laboratory, Radar studies of the moon, Final Rept., Contract NSR 22-009-106, vol. 1, Lexington, Mass., 1967.

Phillips, R. J., Dipole radiation in the lunar environment, Space Sciences Lab., Rept. No. 295, Univ. of Calif., Berkeley, 1968.

Tyler, G. L., Oblique-scattering radar reflectivity of the lunar surface: preliminary results from Explorer 35, J. Geophys. Res., 73, 24, 7609, 1968.

Wait, J. R., Transmission and reflection of electromagnetic waves in the presence of stratified media, J. Res. NBS, 61, 3, 205, 1968.

Ward, S. H., Gross estimates of the conductivity, dielectric constant, and magnetic permeability distributions in the moon, Radio Sci., 4, 2, 117, 1969.

Ward, S. H., G. R. Jiracek, and W. I. Linlor, Electromagnetic reflection from a plane-layered lunar model, J. Geophys. Res., 73, 4, 1355, 1968.

Ward, S. H., G. R. Jiracek, and W. I. Linlor, Some factors affecting electromagnetic detection of lunar subsurface water, IEEE Trans., Geos. Elect., GE-7, 1, 19, 1969.

List of Figures

Figure 14. Reflection coefficient versus frequency at normal incidence for the layered lunar model shown.

Figure 15. Parallel reflection coefficient and apparent dielectric constant versus incident angle at 136.11 MHz showing the dependence upon debris thickness.

Figure 16. Phase of the parallel reflection coefficient and apparent conductivity versus incident angle at 136.11 MHz showing the dependence upon debris thickness.

Figure 17. Parallel and perpendicular reflection coefficient and apparent dielectric constant versus incident angle at 136.11 MHz with a gradational debris layer.

Figure 18. Parallel and perpendicular reflection coefficient and apparent dielectric constant versus incident angle at 136.11 MHz showing the effect of change in magnetic permeability.

Figure 19. Idealized bistatic-radar reflectivity results at 138.11 MHz from a hypothesized lunar profile.

Figure 20. Bistatic-radar reflectivity results at 138.11 MHz when considering the mean return from a uniform distribution of debris depth over the range 0 to 10 m.

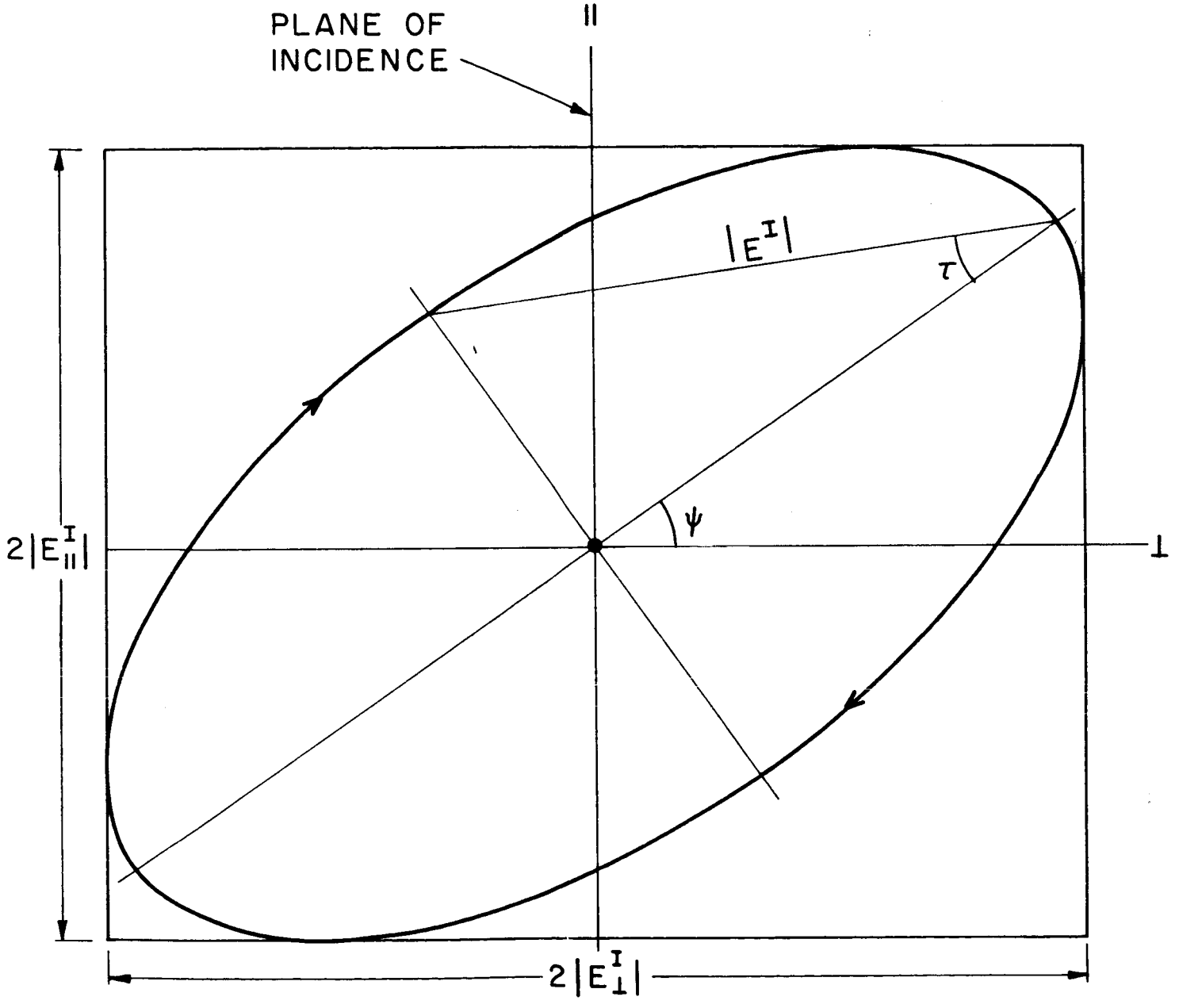

Figure 1

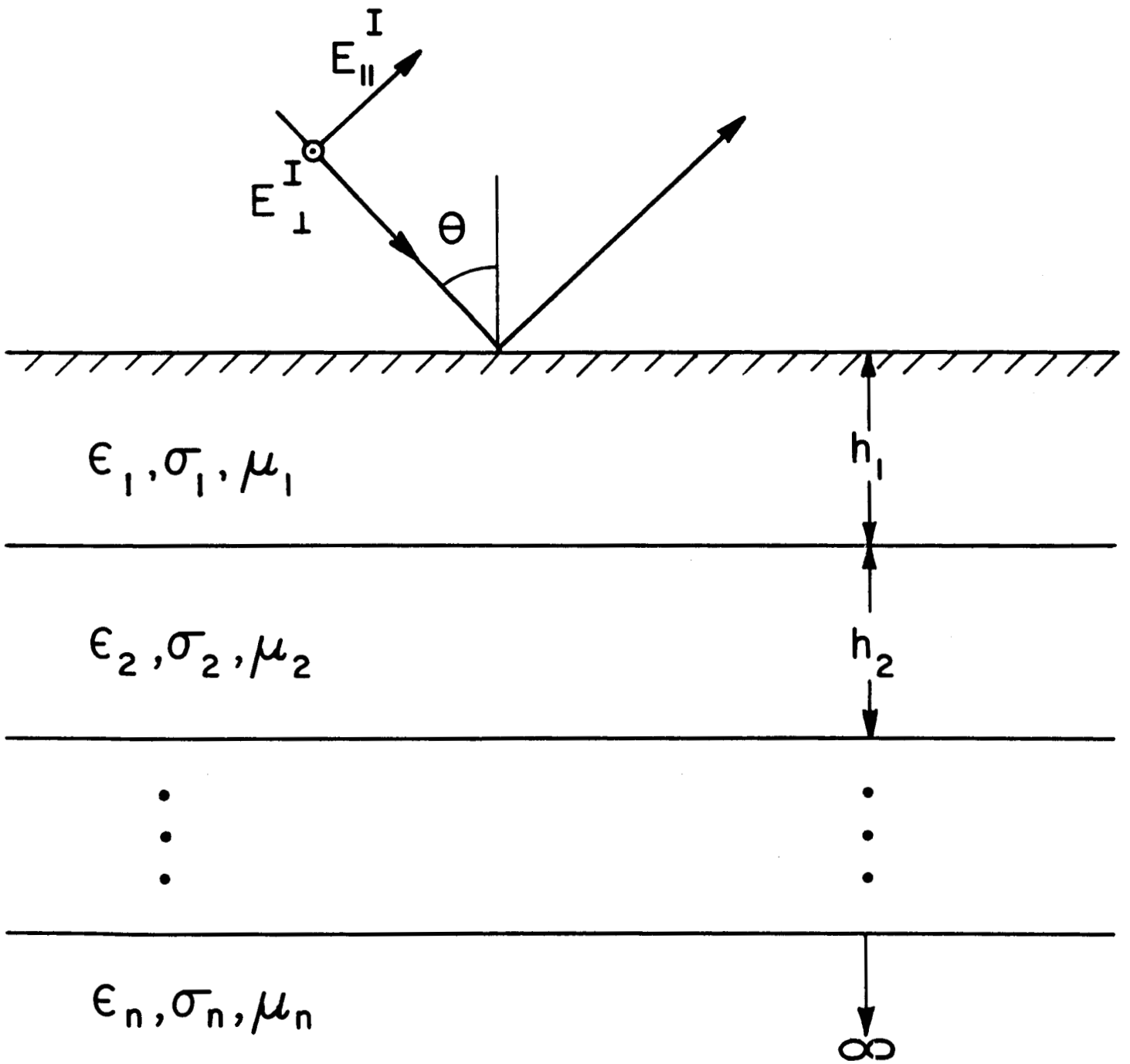
I
$E_{\parallel}$
I
$E_{\perp}$
θ
$\epsilon_1, \sigma_1, \mu_1$
h_1
$\epsilon_2, \sigma_2, \mu_2$
h_2
$\epsilon_n, \sigma_n, \mu_n$
∞

Figure 2

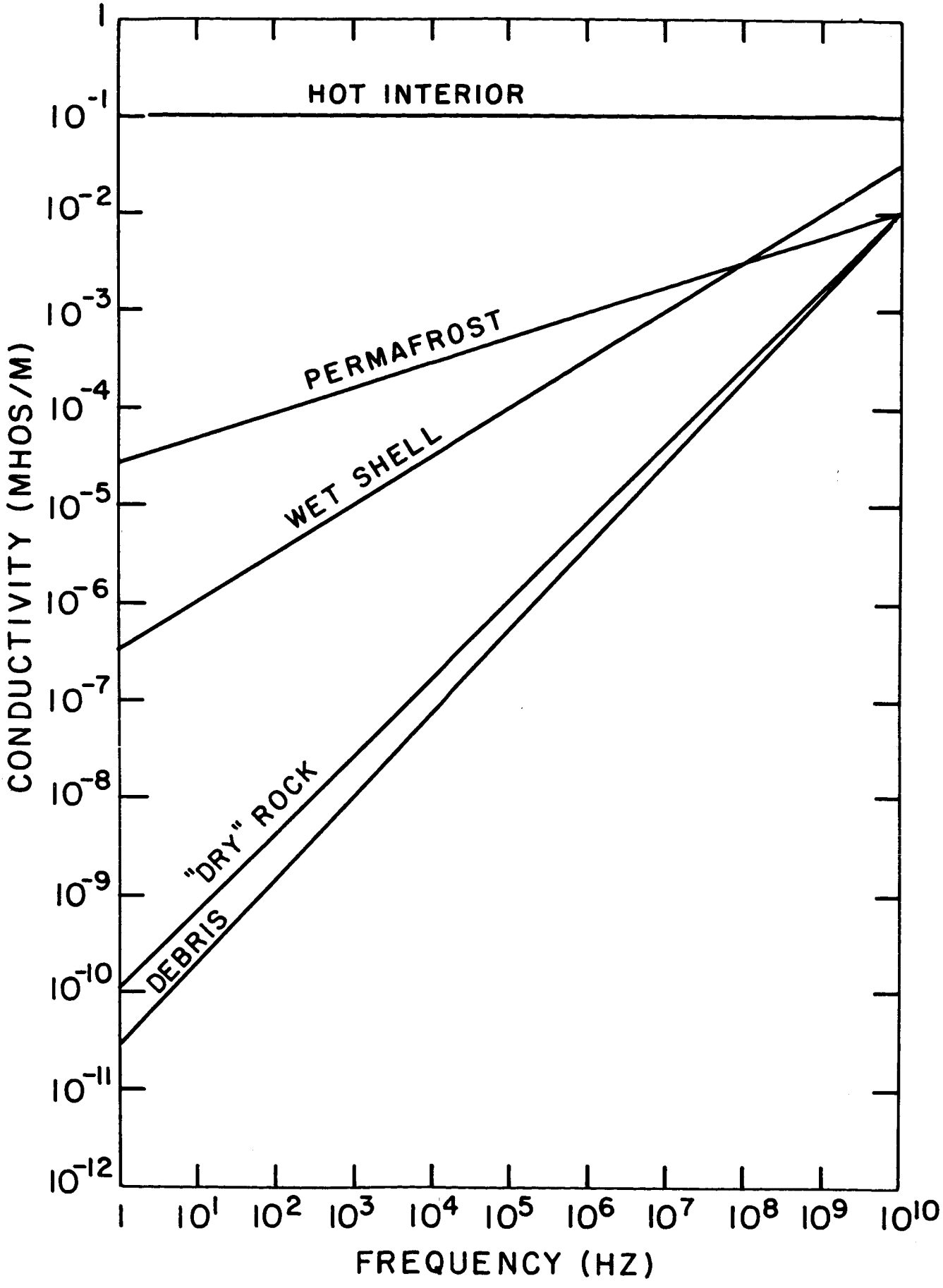
HOT INTERIOR
PERMAFROST
WET SHELL
"DRY" ROCK
DEBRIS
CONDUCTIVITY (MHOS/M)
FREQUENCY (HZ)
1
10^-1
10^-2
10^-3
10^-4
10^-5
10^-6
10^-7
10^-8
10^-9
10^-10
10^-11
10^-12
1
10^1
10^2
10^3
10^4
10^5
10^6
10^7
10^8
10^9
10^10

Figure 3

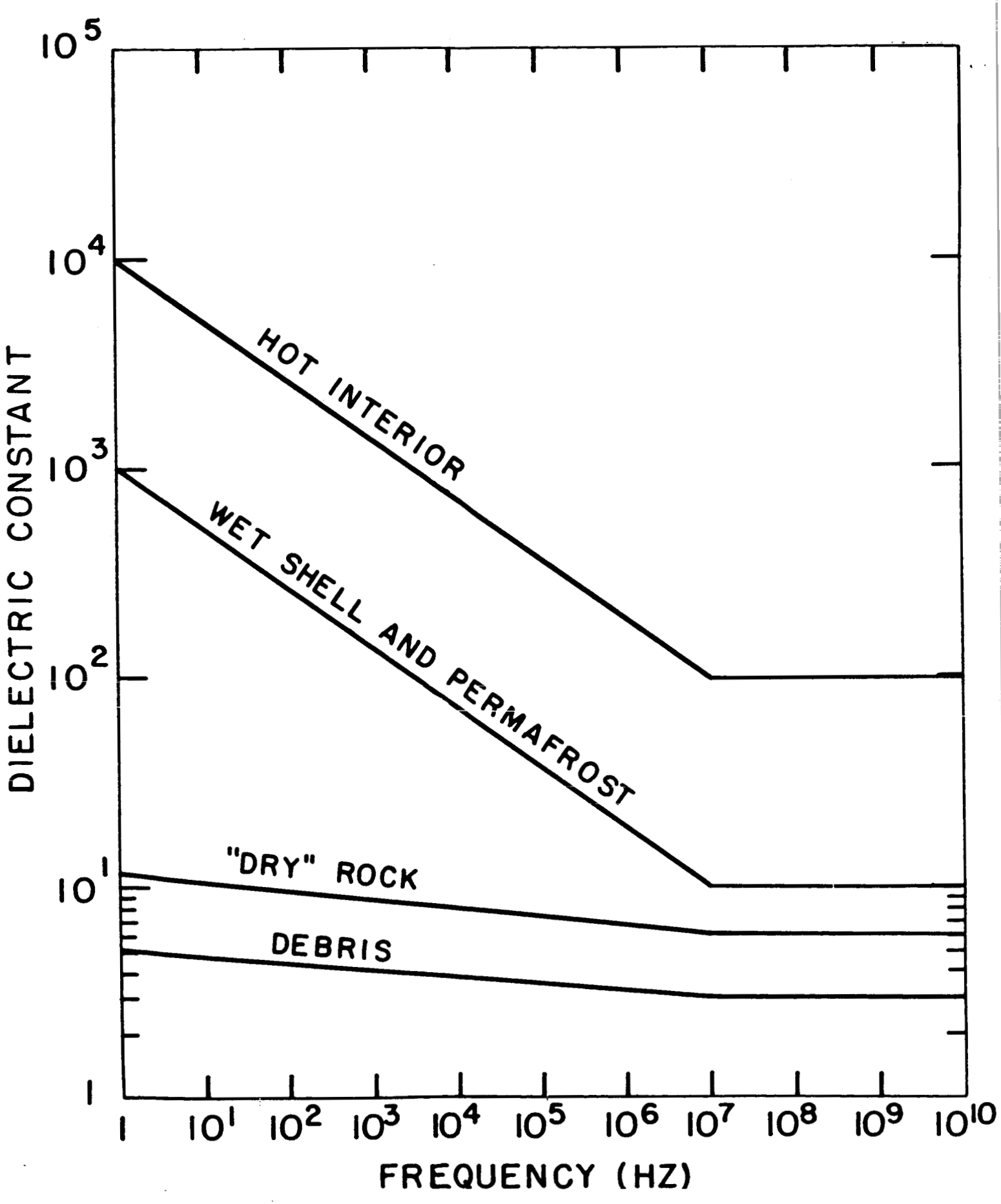
DIELECTRIC CONSTANT
10^5
10^4
10^3
10^2
10^1
1
HOT INTERIOR
WET SHELL AND PERMAFROST
"DRY" ROCK
DEBRIS
1
10^1
10^2
10^3
10^4
10^5
10^6
10^7
10^8
10^9
10^{10}
FREQUENCY (HZ)

Figure 4

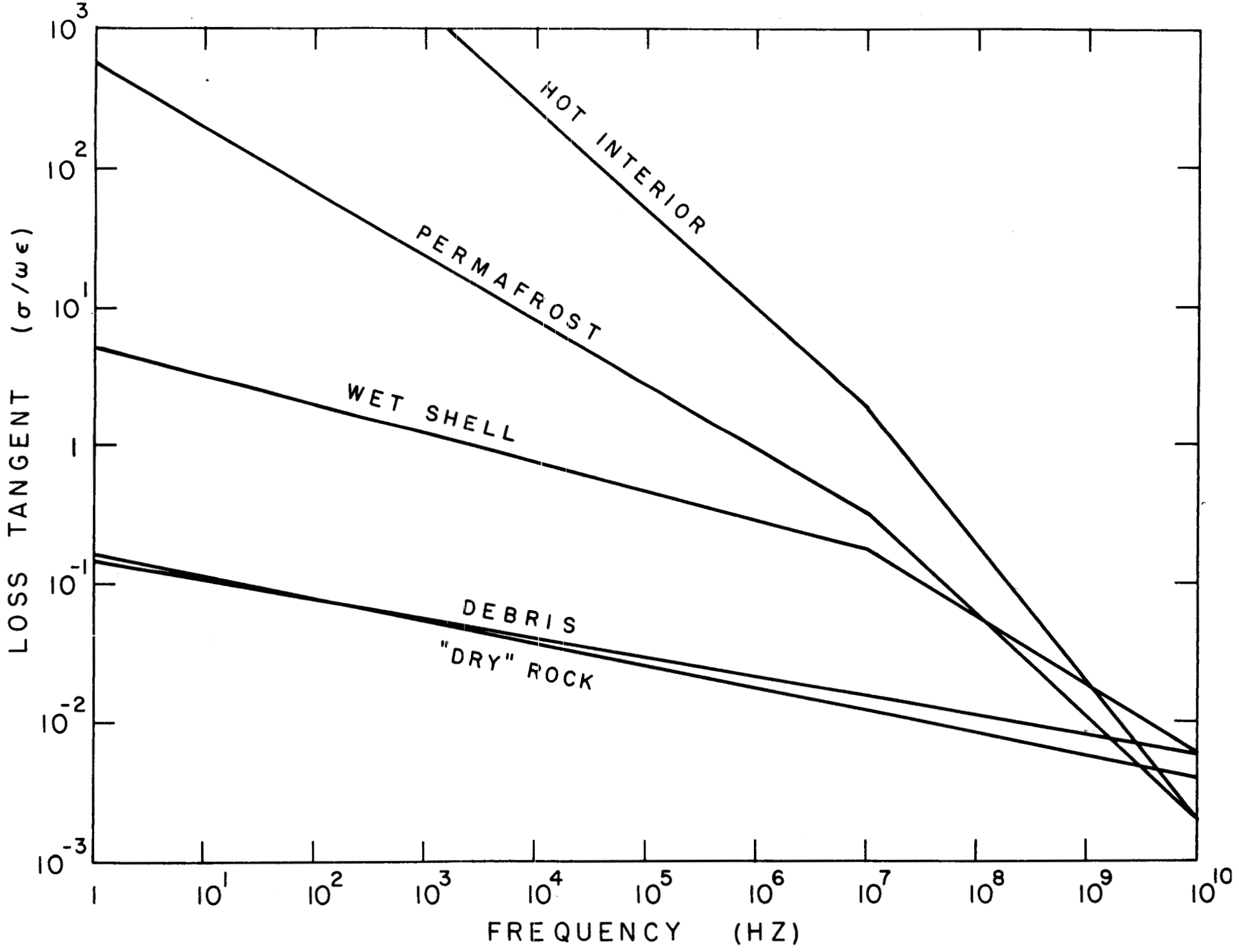
HOT INTERIOR
PERMAFROST
WET SHELL
DEBRIS
"DRY" ROCK
LOSS TANGENT (σ/ωε)
FREQUENCY (HZ)
10^3
10^2
10^1
1
10^-1
10^-2
10^-3
1
10^1
10^2
10^3
10^4
10^5
10^6
10^7
10^8
10^9
10^10

Figure 5

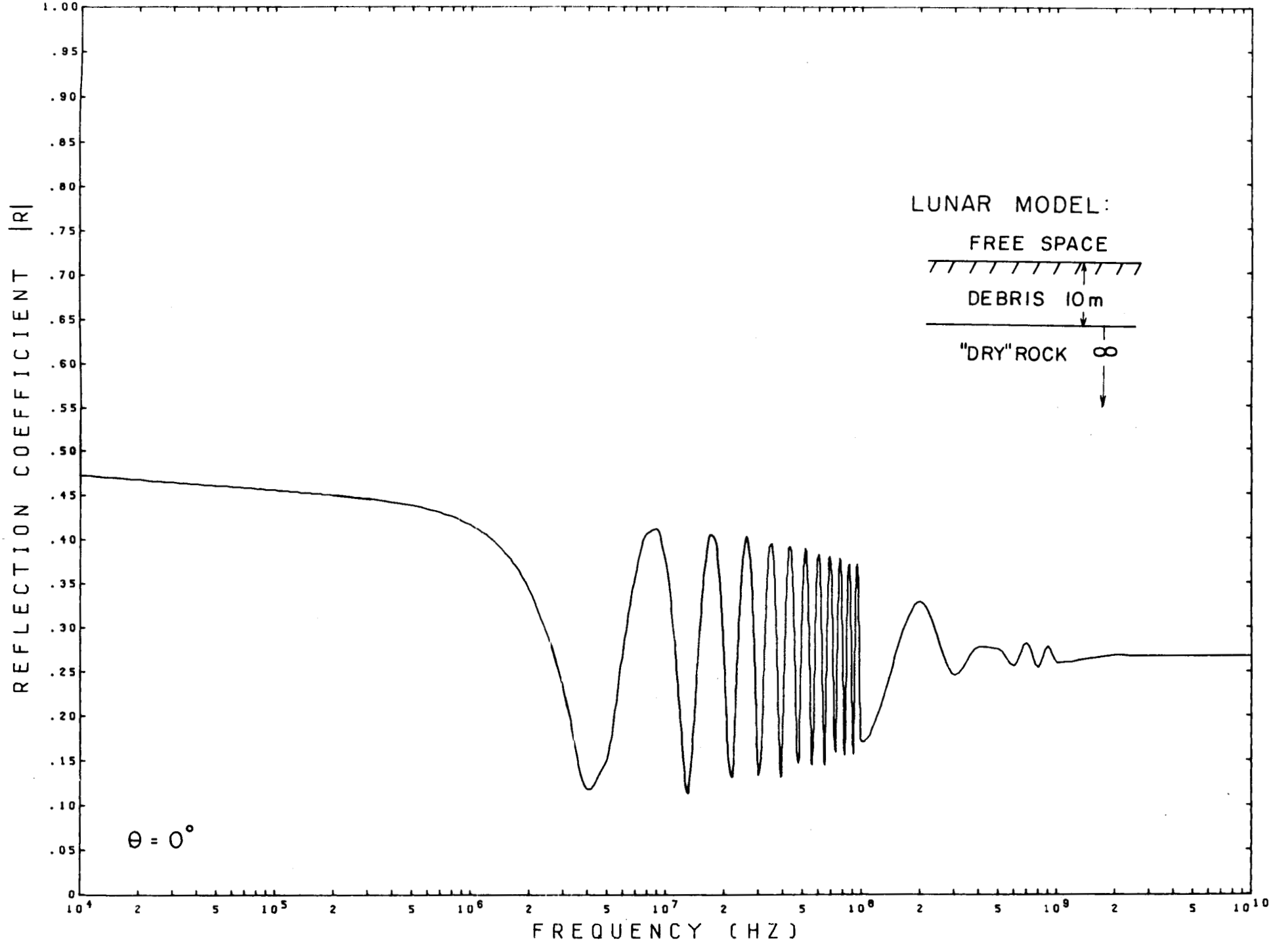
LUNAR MODEL:
FREE SPACE
DEBRIS 10m
"DRY" ROCK ∞
Θ = 0°
REFLECTION COEFFICIENT |R|
FREQUENCY (HZ)
1.00
.95
.90
.85
.80
.75
.70
.65
.60
.55
.50
.45
.40
.35
.30
.25
.20
.15
.10
.05
0
10⁴
2
5
10⁵
2
5
10⁶
2
5
10⁷
2
5
10⁸
2
5
10⁹
2
5
10¹⁰

Figure 6

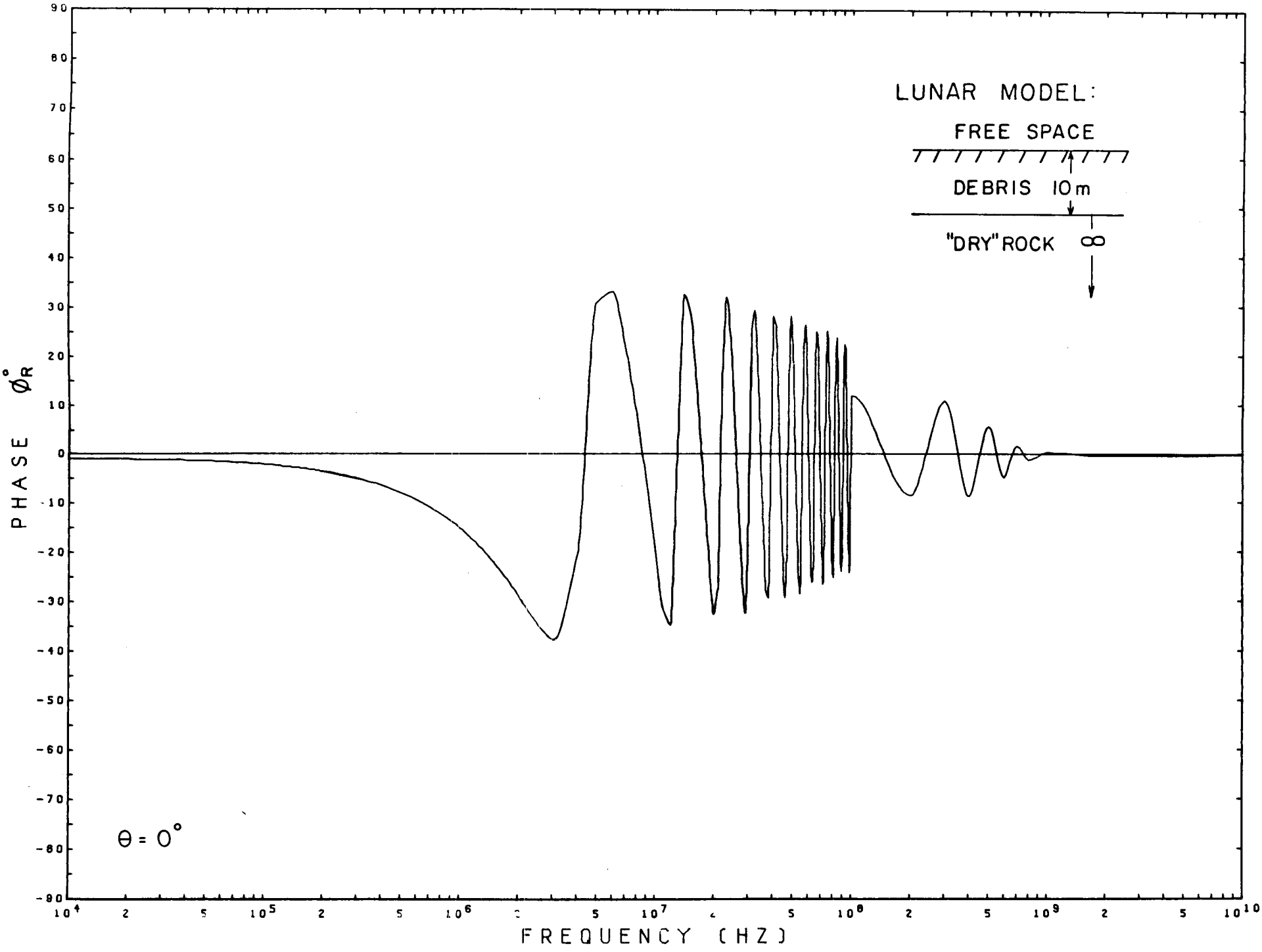
LUNAR MODEL:
FREE SPACE
DEBRIS 10m
"DRY" ROCK
∞
PHASE ϕ_R°
$\theta = 0^\circ$
FREQUENCY (HZ)
90
80
70
60
50
40
30
20
10
0
-10
-20
-30
-40
-50
-60
-70
-80
-90
10^4
2
5
10^5
2
5
10^6
5
10^7
5
10^8
2
5
10^9
2
5
10^{10}

Figure 7

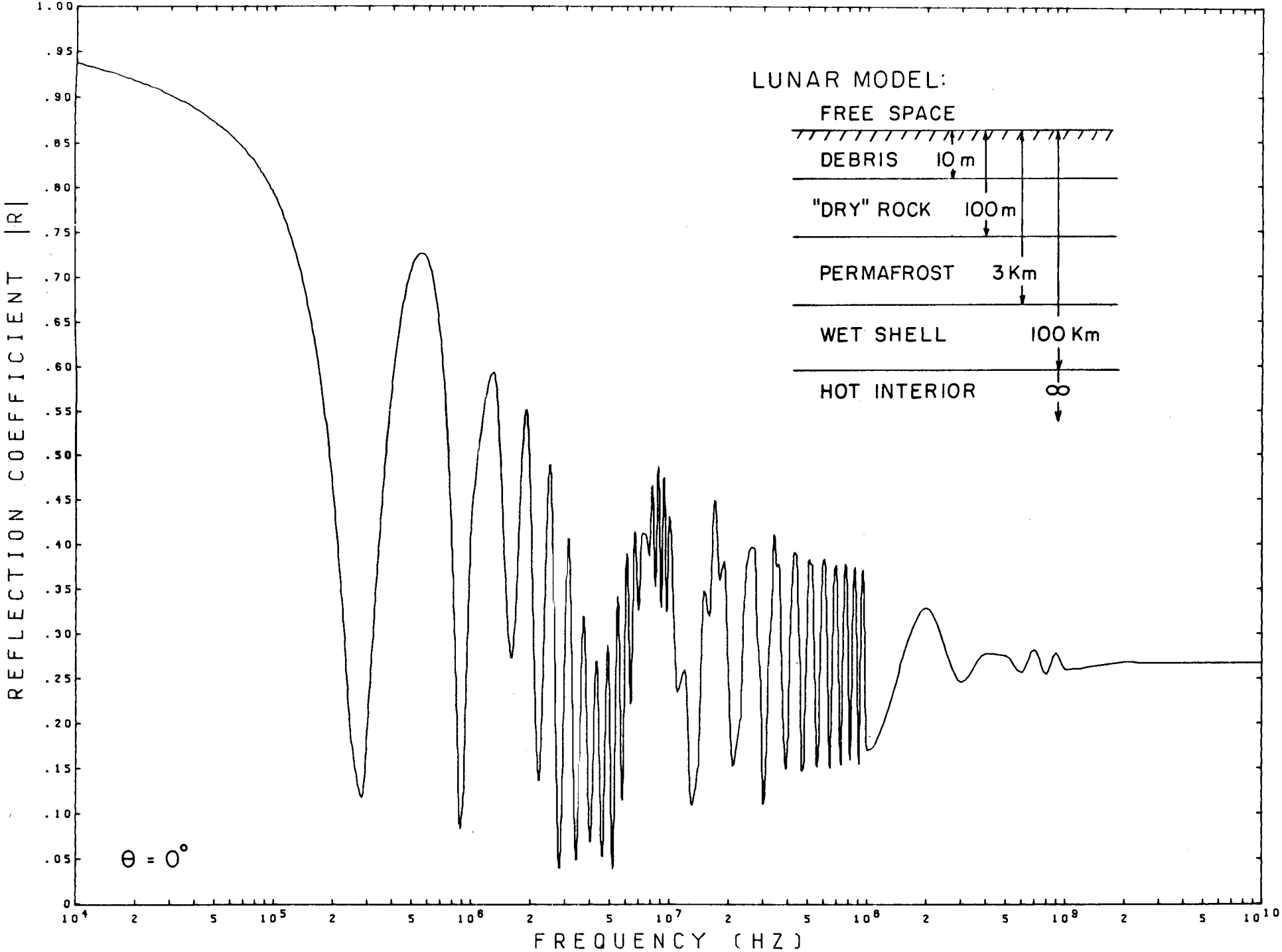
LUNAR MODEL:
FREE SPACE
DEBRIS 10 m
"DRY" ROCK 100 m
PERMAFROST 3 Km
WET SHELL 100 Km
HOT INTERIOR ∞
REFLECTION COEFFICIENT |R|
1.00
.95
.90
.85
.80
.75
.70
.65
.60
.55
.50
.45
.40
.35
.30
.25
.20
.15
.10
.05
0
θ = 0°
10^4 2 5 10^5 2 5 10^6 2 5 10^7 2 5 10^8 2 5 10^9 2 5 10^10
FREQUENCY (HZ)

Figure 8

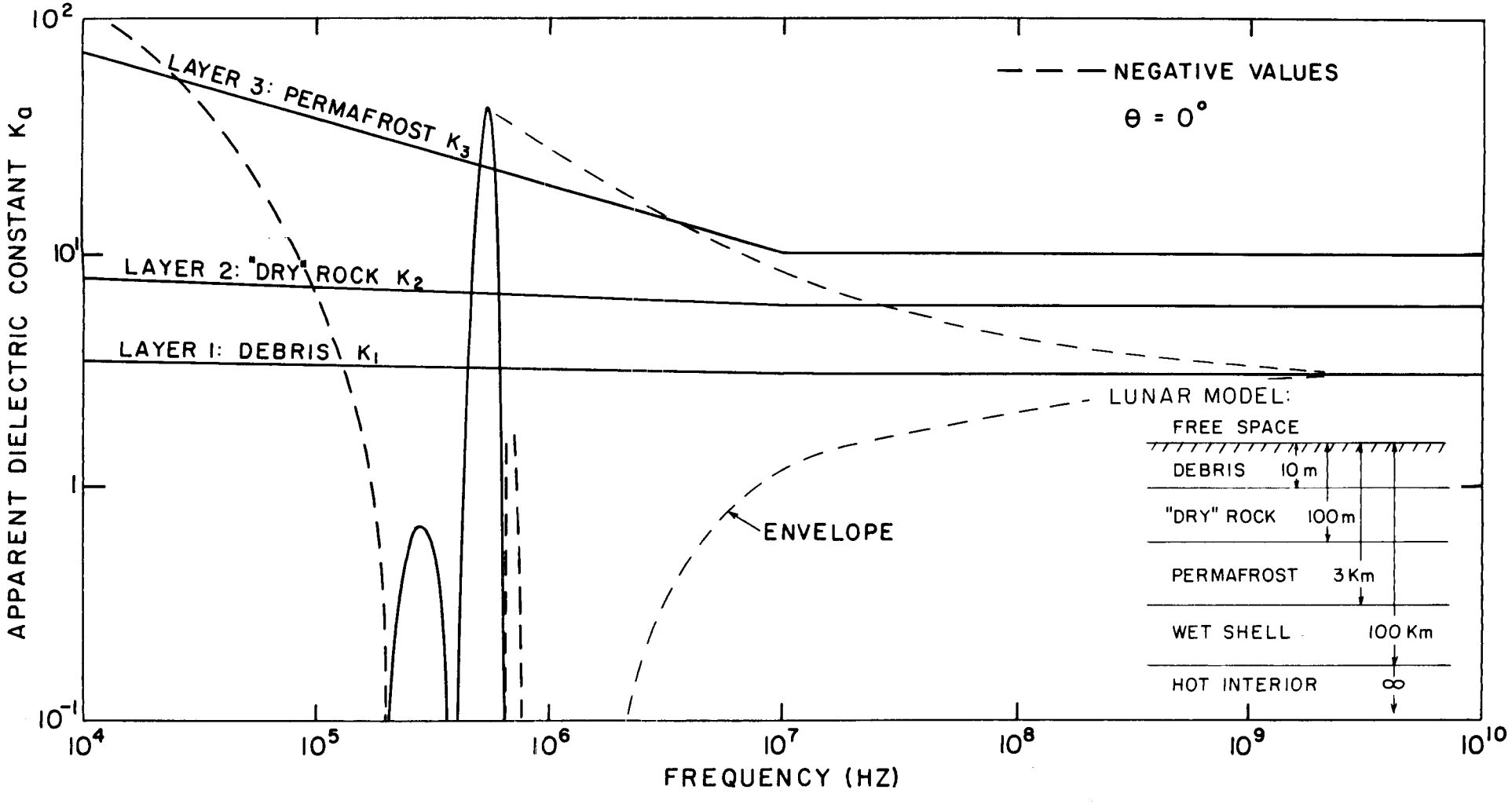
APPARENT DIELECTRIC CONSTANT K_a
10^2
10^1
1
10^{-1}
10^4
10^5
10^6
10^7
10^8
10^9
10^{10}
FREQUENCY (HZ)
LAYER 3: PERMAFROST K_3
LAYER 2: "DRY" ROCK K_2
LAYER 1: DEBRIS K_1
NEGATIVE VALUES
$\theta = 0°$
LUNAR MODEL:
FREE SPACE
DEBRIS 10 m
"DRY" ROCK 100 m
PERMAFROST 3 Km
WET SHELL 100 Km
HOT INTERIOR ∞
ENVELOPE

Figure 9

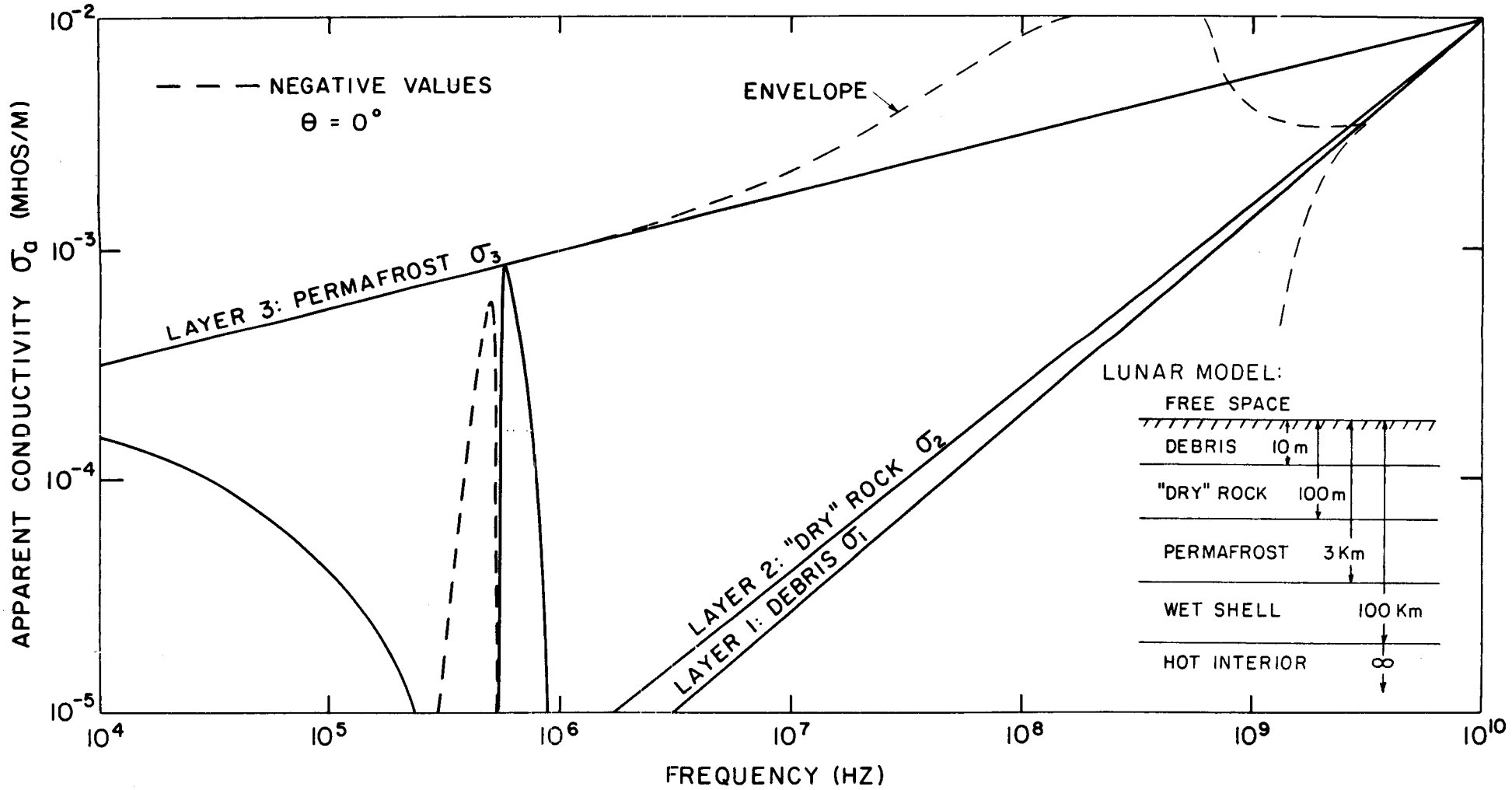
APPARENT CONDUCTIVITY σ_a (MHOS/M)
10^{-2}
10^{-3}
10^{-4}
10^{-5}
— — — NEGATIVE VALUES
$\theta = 0°$
ENVELOPE
LAYER 3: PERMAFROST σ_3
LAYER 2: "DRY" ROCK σ_2
LAYER 1: DEBRIS σ_1
LUNAR MODEL:
FREE SPACE
DEBRIS 10 m
"DRY" ROCK 100 m
PERMAFROST 3 Km
WET SHELL 100 Km
HOT INTERIOR ∞
10^4
10^5
10^6
10^7
10^8
10^9
10^{10}
FREQUENCY (HZ)

Figure 10

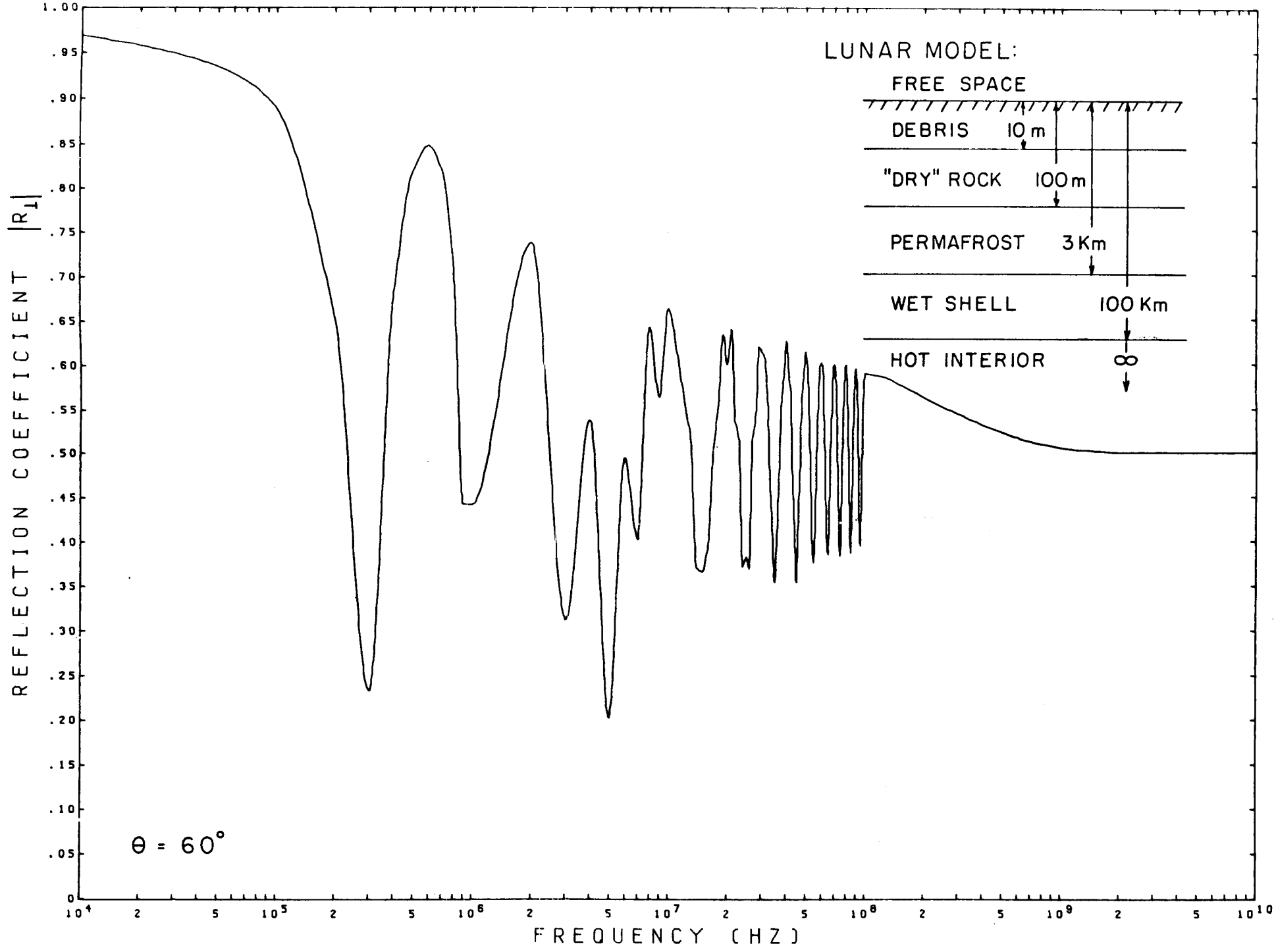
LUNAR MODEL:
FREE SPACE
DEBRIS
10 m
"DRY" ROCK
100 m
PERMAFROST
3 Km
WET SHELL
100 Km
HOT INTERIOR
∞
θ = 60°
REFLECTION COEFFICIENT |R⊥|
FREQUENCY (HZ)
1.00
.95
.90
.85
.80
.75
.70
.65
.60
.55
.50
.45
.40
.35
.30
.25
.20
.15
.10
.05
0
10⁴
2
5
10⁵
2
5
10⁶
2
5
10⁷
2
5
10⁸
2
5
10⁹
2
5
10¹⁰

Figure 11

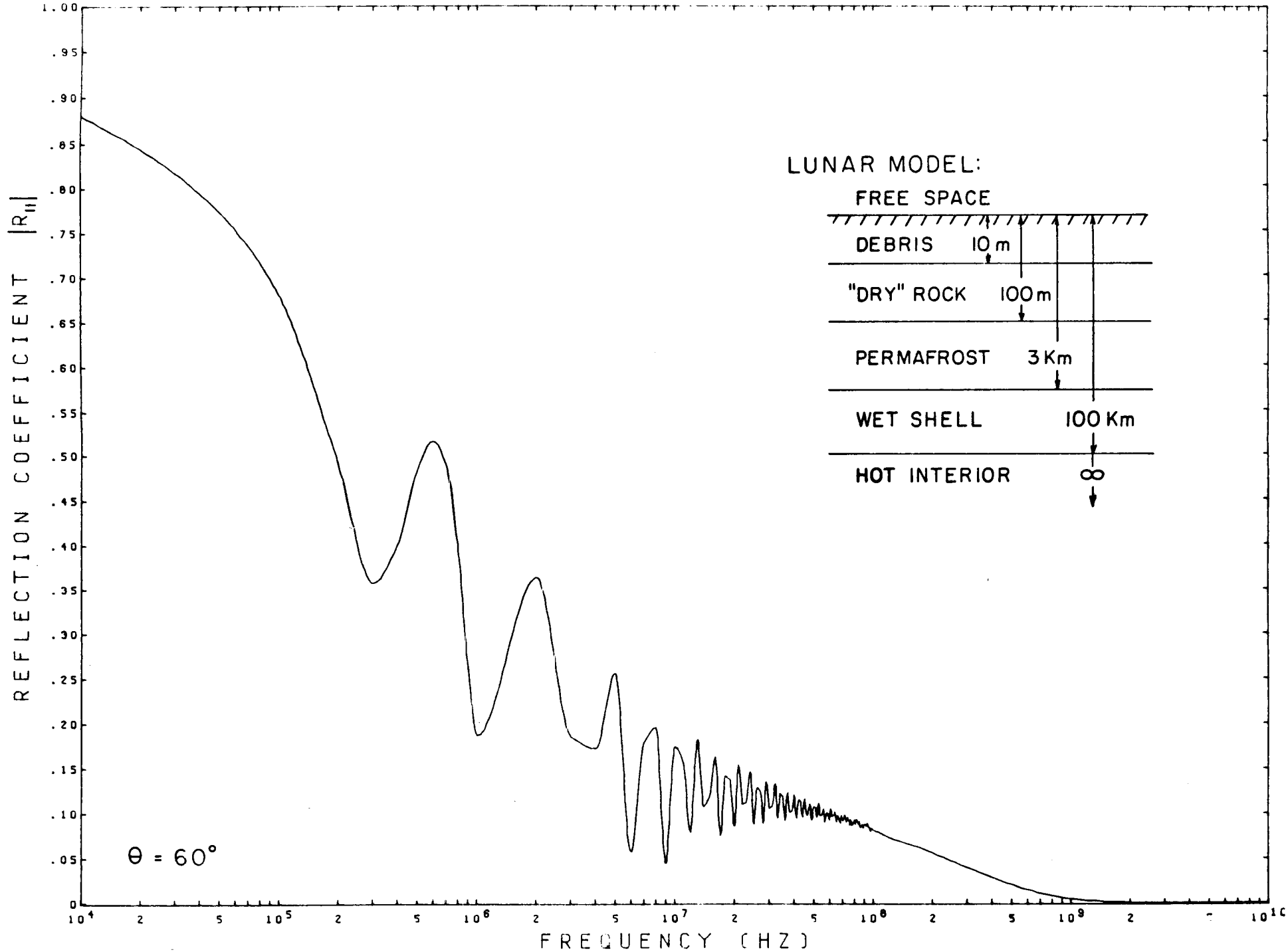
REFLECTION COEFFICIENT |R⊥|
1.00
.95
.90
.85
.80
.75
.70
.65
.60
.55
.50
.45
.40
.35
.30
.25
.20
.15
.10
.05
0
θ = 60°
10⁴ 2 5 10⁵ 2 5 10⁶ 2 5 10⁷ 2 5 10⁸ 2 5 10⁹ 2 10¹⁰
FREQUENCY (HZ)
LUNAR MODEL:
FREE SPACE
DEBRIS 10 m
"DRY" ROCK 100 m
PERMAFROST 3 Km
WET SHELL 100 Km
HOT INTERIOR ∞

Figure 12

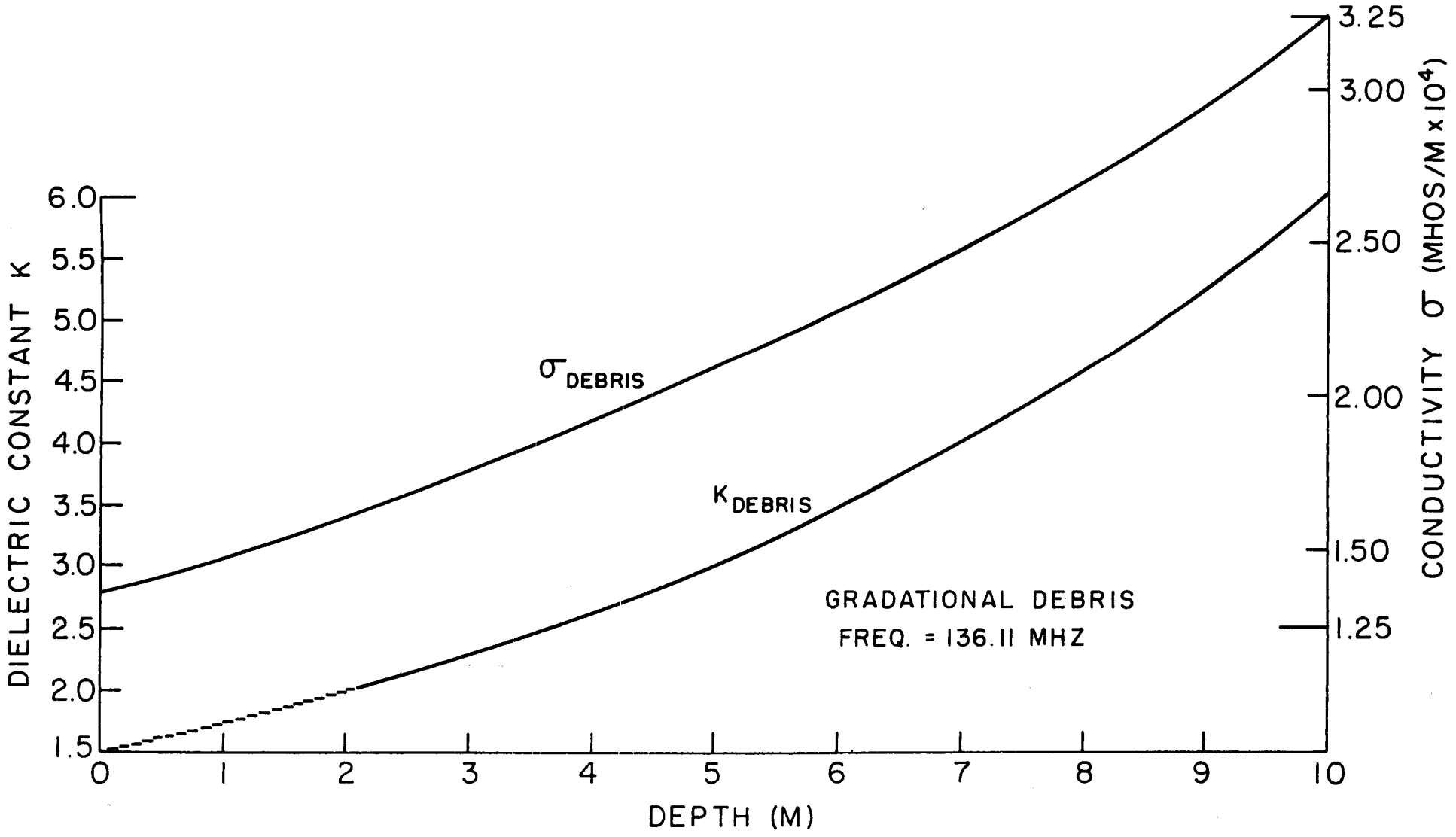
DIELECTRIC CONSTANT K
6.0
5.5
5.0
4.5
4.0
3.5
3.0
2.5
2.0
1.5
0
1
2
3
4
5
6
7
8
9
10
DEPTH (M)
3.25
3.00
2.50
2.00
1.50
1.25
CONDUCTIVITY σ (MHOS/M x 10⁴)
σ DEBRIS
K DEBRIS
GRADATIONAL DEBRIS
FREQ. = 136.11 MHZ

Figure 13

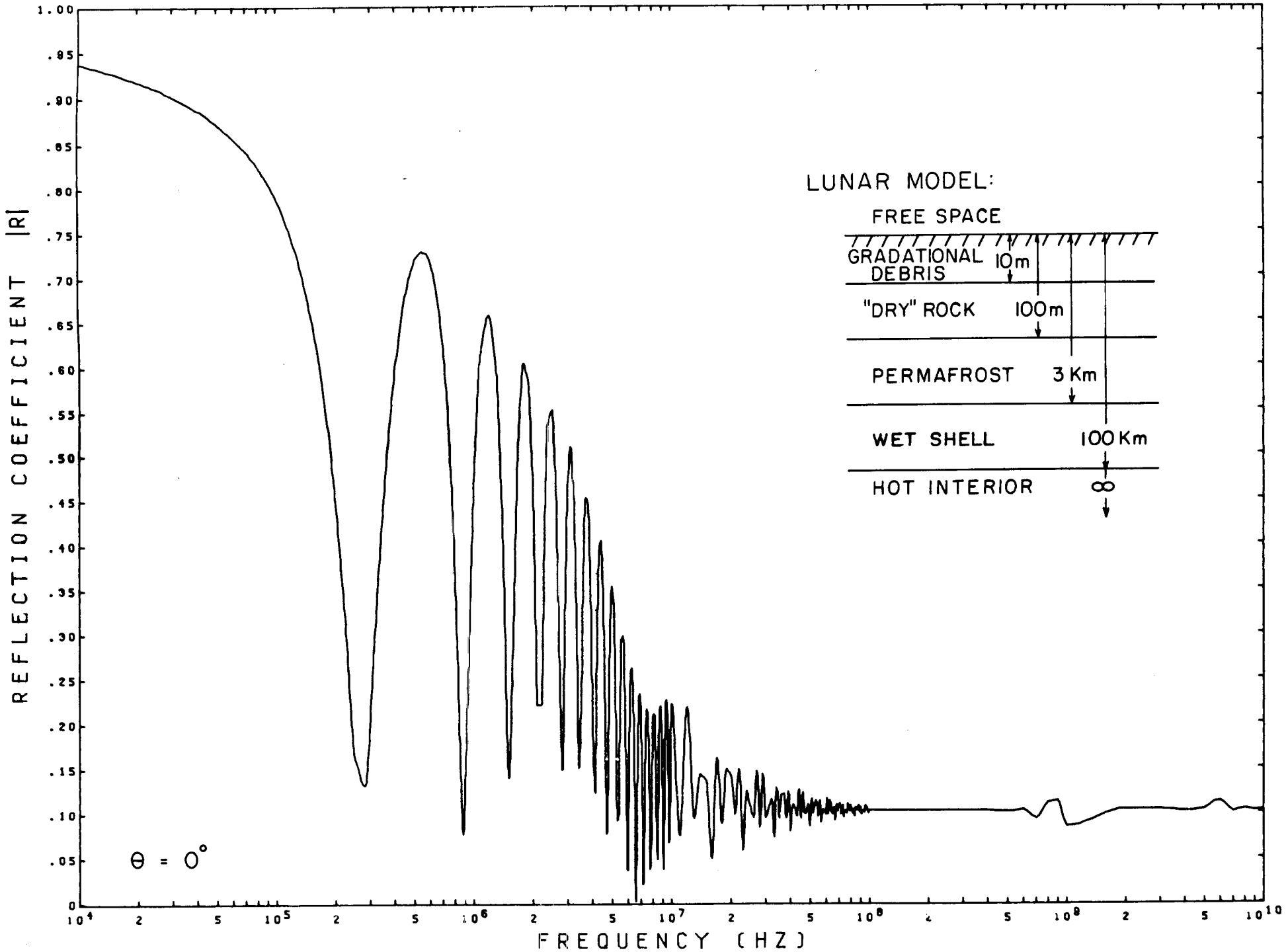
REFLECTION COEFFICIENT |R|
1.00
.95
.90
.85
.80
.75
.70
.65
.60
.55
.50
.45
.40
.35
.30
.25
.20
.15
.10
.05
0
θ = 0°
10^4 2 5 10^5 2 5 10^6 2 5 10^7 2 5 10^8 2 5 10^9 2 5 10^10
FREQUENCY (HZ)
LUNAR MODEL:
FREE SPACE
GRADATIONAL DEBRIS
10m
"DRY" ROCK
100m
PERMAFROST
3 Km
WET SHELL
100 Km
HOT INTERIOR
∞

Figure 14

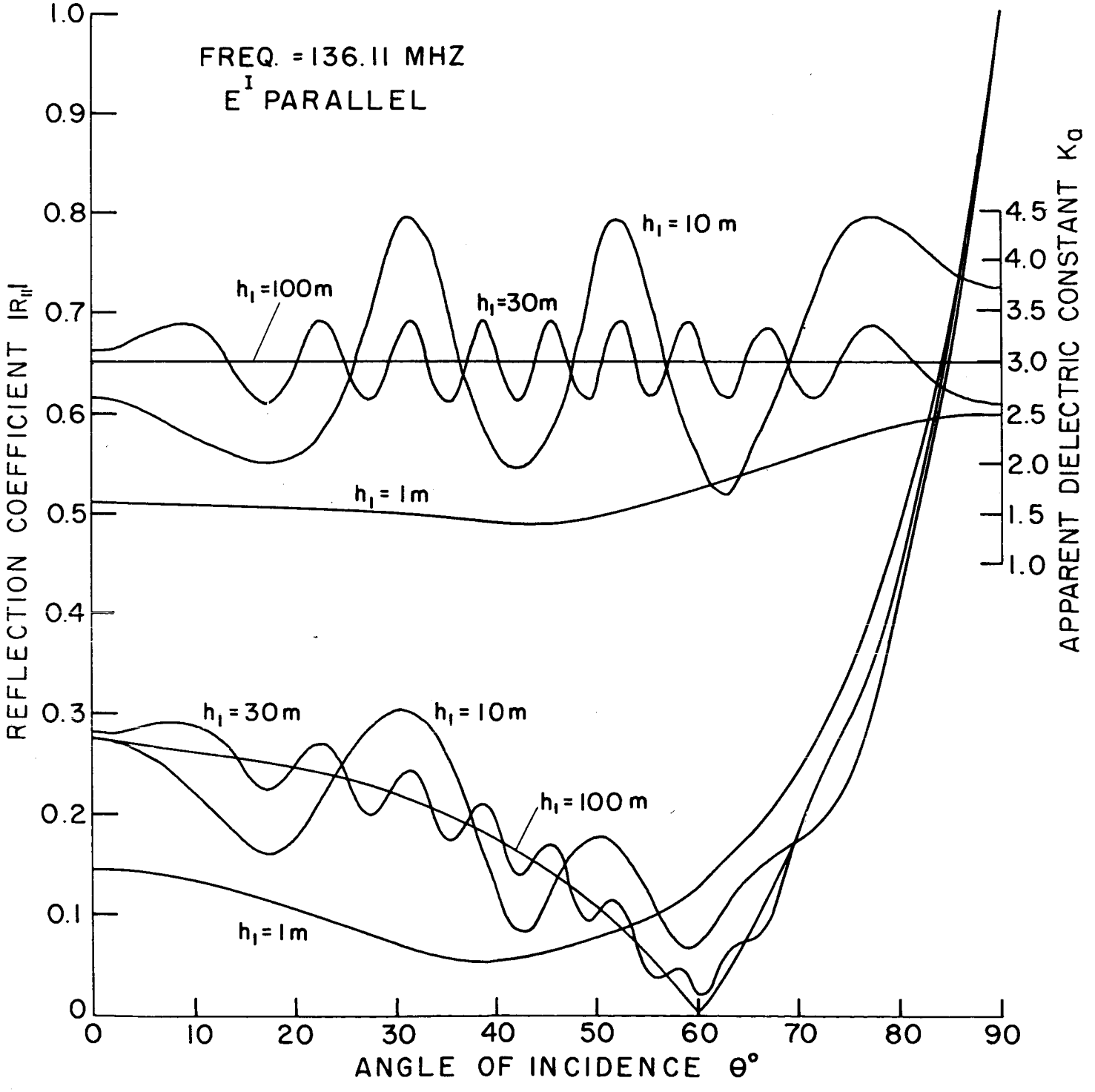
FREQ. = 136.11 MHZ
E^I PARALLEL
h1 = 10 m
h1 =100m
h1=30m
h1 = 1m
h1 = 30m
h1 = 10m
h1 = 100 m
h1 = 1m
REFLECTION COEFFICIENT |R||
APPARENT DIELECTRIC CONSTANT Ka
ANGLE OF INCIDENCE θ°
1.0
0.9
0.8
0.7
0.6
0.5
0.4
0.3
0.2
0.1
0
4.5
4.0
3.5
3.0
2.5
2.0
1.5
1.0
0
10
20
30
40
50
60
70
80
90

Figure 15

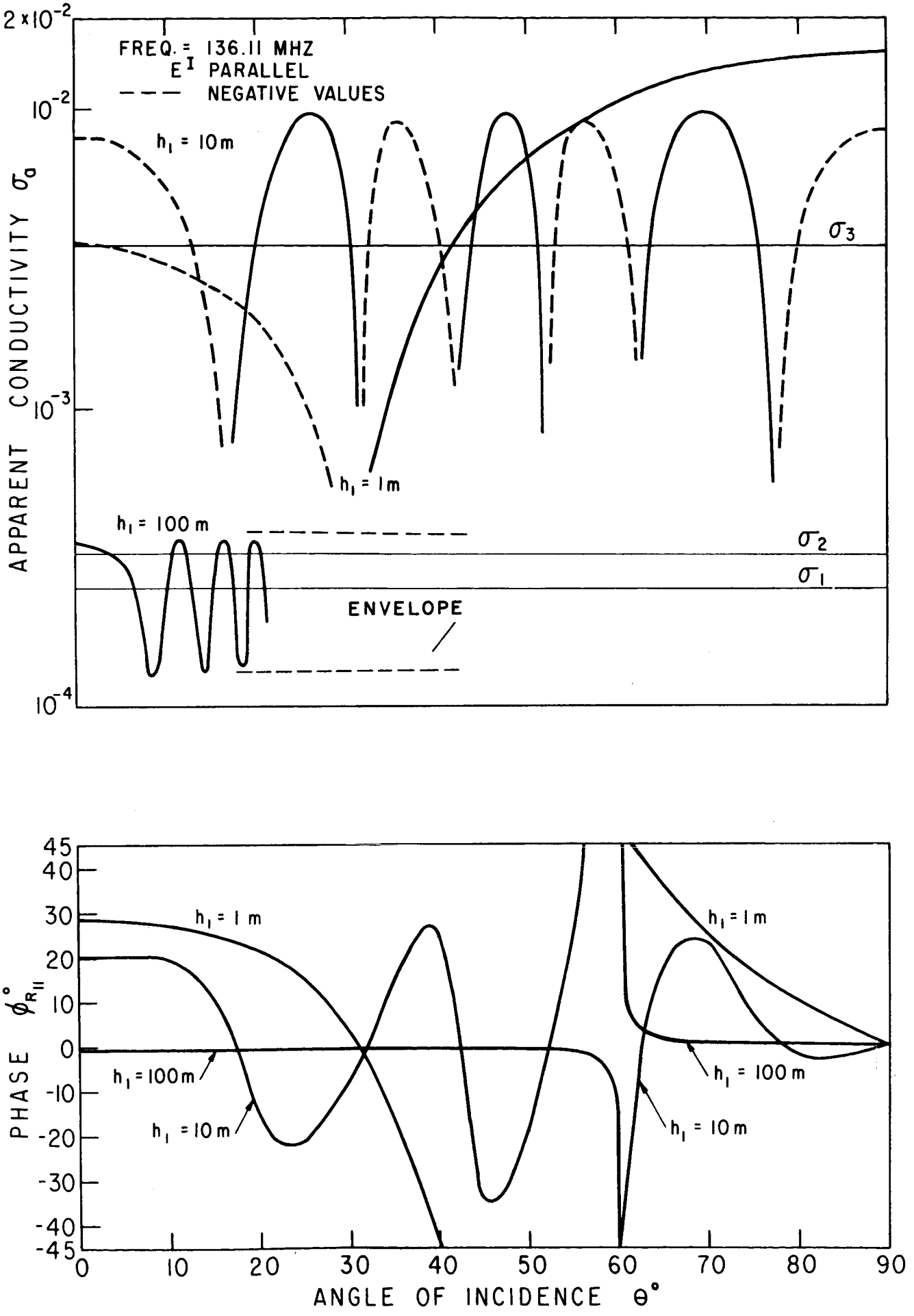
FREQ. = 136.11 MHZ
E^I PARALLEL
NEGATIVE VALUES
APPARENT CONDUCTIVITY σa
2x10^-2
10^-2
10^-3
10^-4
h1 = 10m
h1 = 1m
h1 = 100 m
σ3
σ2
σ1
ENVELOPE
PHASE φ°R||
45
40
30
20
10
0
-10
-20
-30
-40
-45
h1 = 1 m
h1 = 100m
h1 = 10m
h1 = 1m
h1 = 100 m
h1 = 10m
0
10
20
30
40
50
60
70
80
90
ANGLE OF INCIDENCE θ°

Figure 16

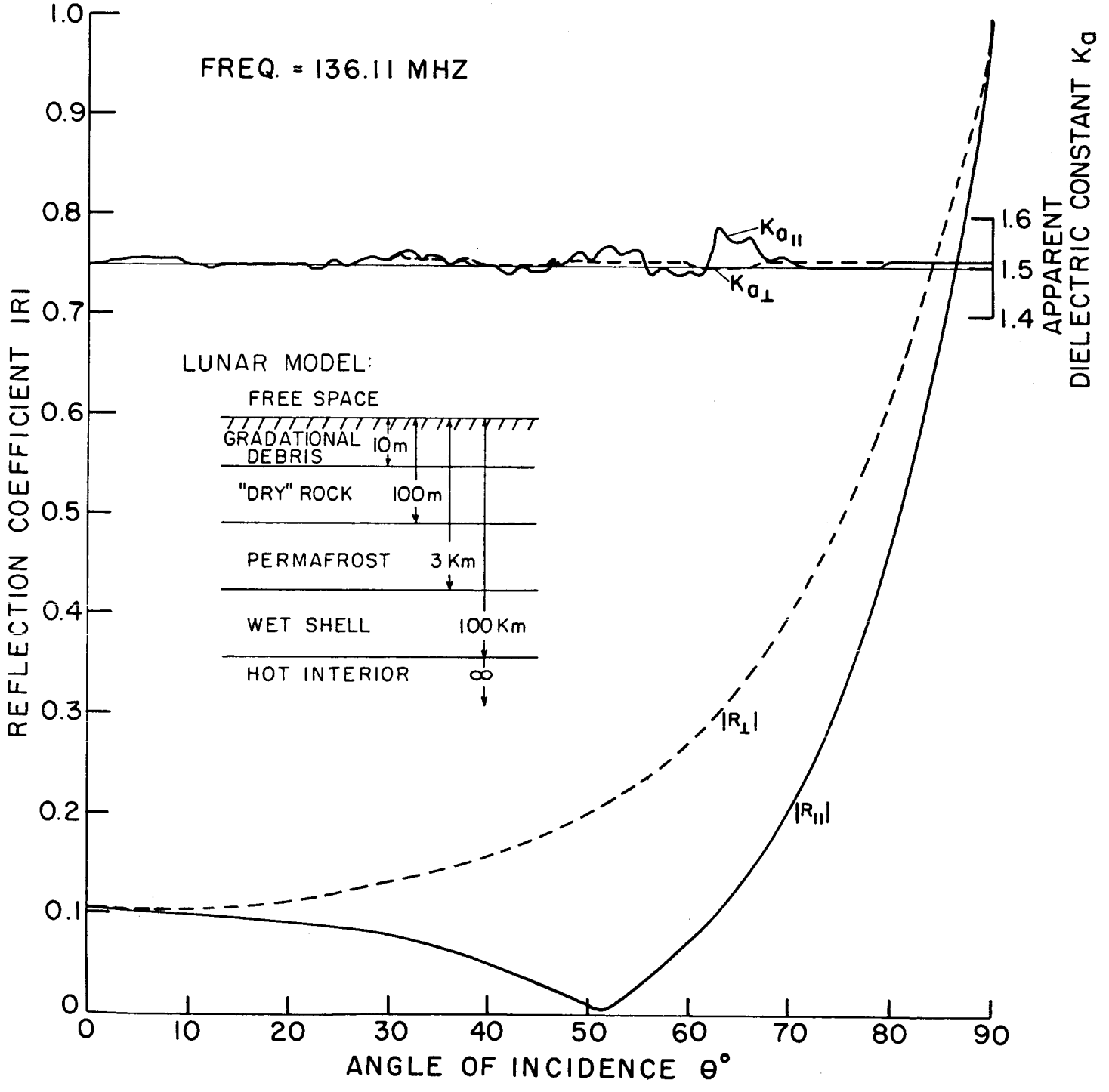
FREQ. = 136.11 MHZ
REFLECTION COEFFICIENT IRI
APPARENT DIELECTRIC CONSTANT Ka
$K_{a_{11}}$
$K_{a_\perp}$
1.6
1.5
1.4
LUNAR MODEL:
FREE SPACE
GRADATIONAL DEBRIS
10m
"DRY" ROCK
100m
PERMAFROST
3 Km
WET SHELL
100 Km
HOT INTERIOR
∞
$|R_\perp|$
$|R_{11}|$
ANGLE OF INCIDENCE θ°

Figure 17

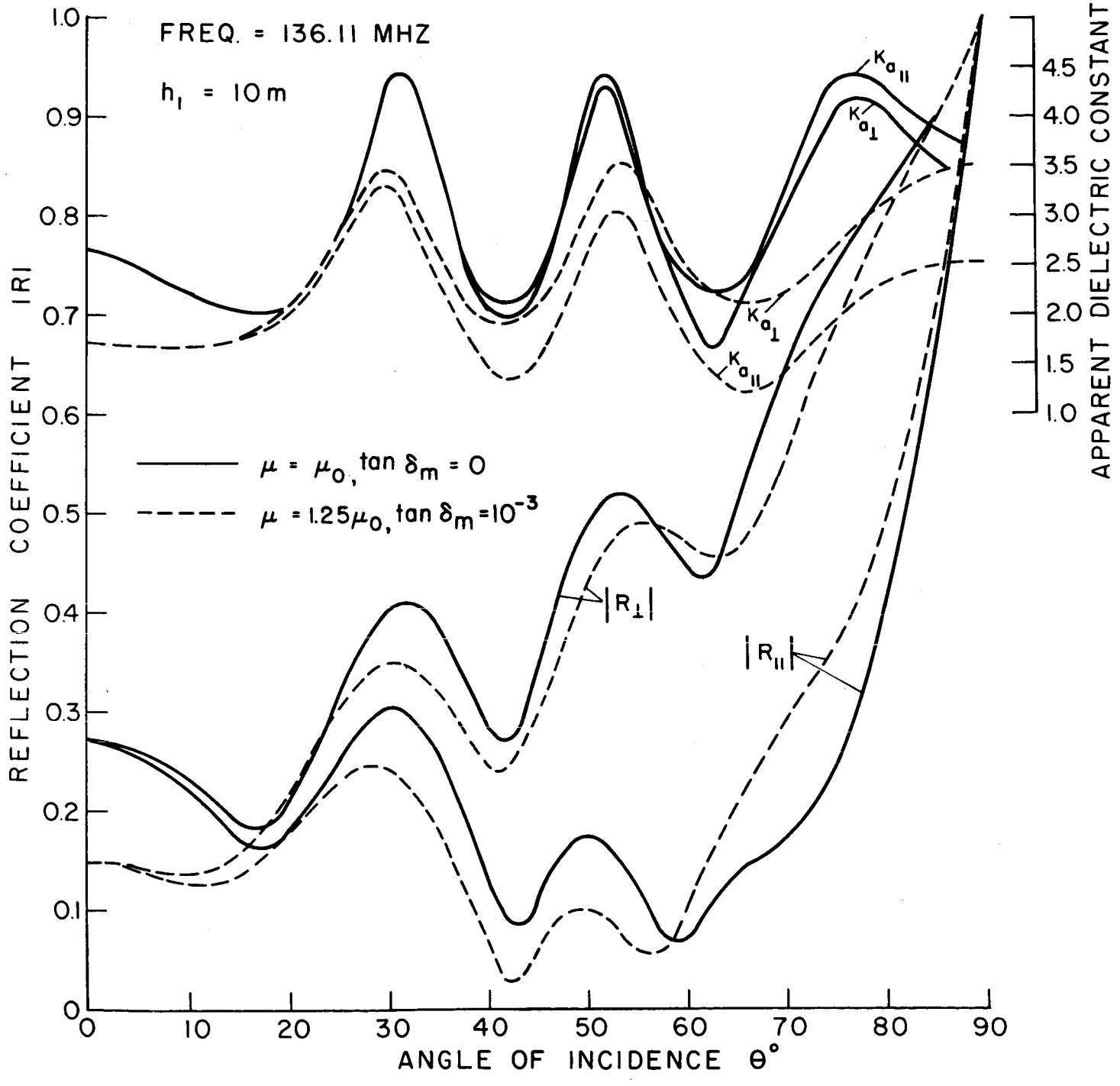
FREQ. = 136.11 MHZ
h_1 = 10 m
$\mu = \mu_0$, tan $\delta_m = 0$
$\mu = 1.25\mu_0$, tan $\delta_m = 10^{-3}$
$K_{a_{11}}$
$K_{a_\perp}$
$|R_\perp|$
$|R_{11}|$
REFLECTION COEFFICIENT IRI
APPARENT DIELECTRIC CONSTANT
ANGLE OF INCIDENCE θ°
0
0.1
0.2
0.3
0.4
0.5
0.6
0.7
0.8
0.9
1.0
1.0
1.5
2.0
2.5
3.0
3.5
4.0
4.5
0
10
20
30
40
50
60
70
80
90

Figure 18

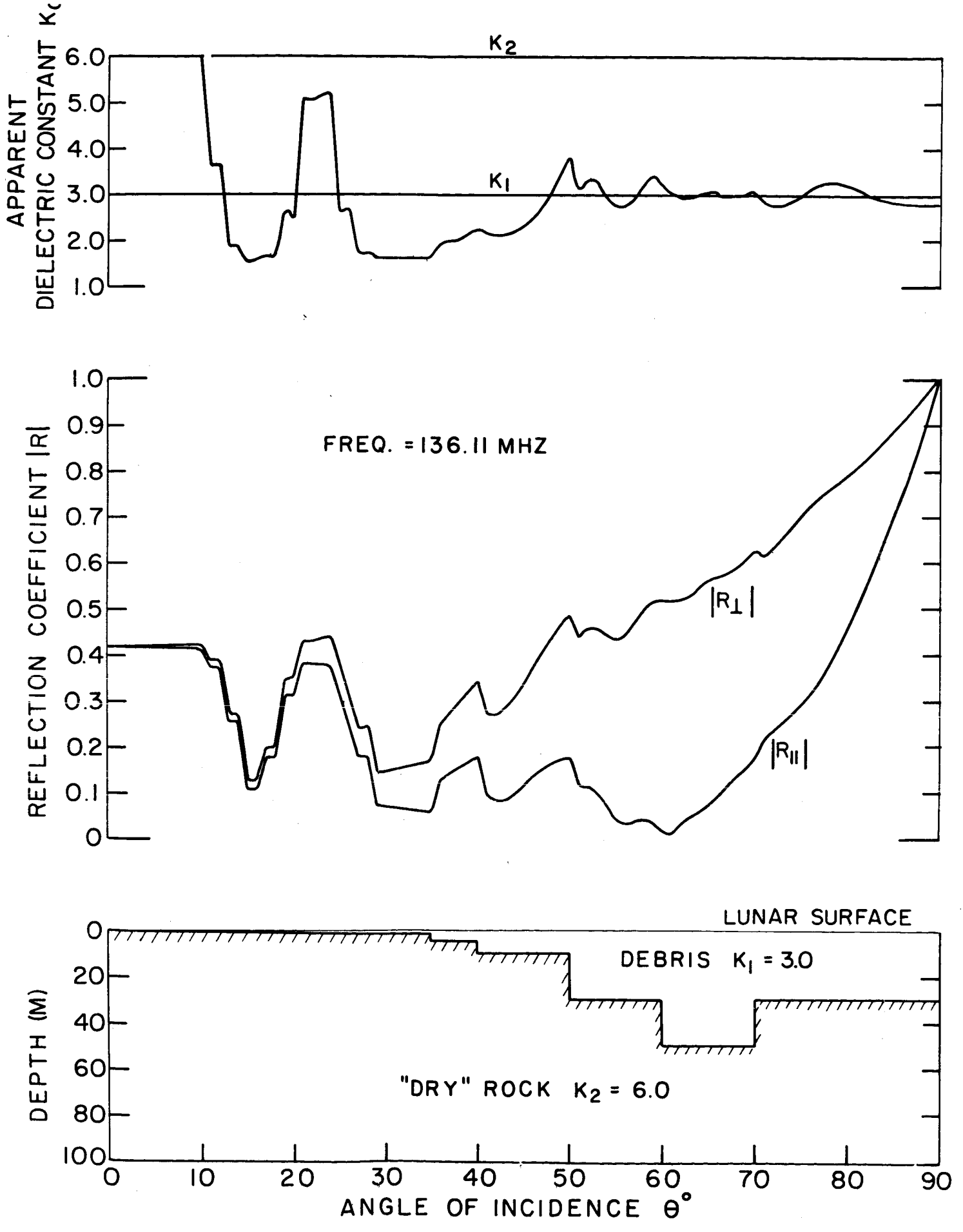
APPARENT DIELECTRIC CONSTANT Kε
6.0
5.0
4.0
3.0
2.0
1.0
K2
K1
REFLECTION COEFFICIENT |R|
1.0
0.9
0.8
0.7
0.6
0.5
0.4
0.3
0.2
0.1
0
FREQ. = 136.11 MHZ
|R⊥|
|R||
LUNAR SURFACE
DEBRIS K1 = 3.0
"DRY" ROCK K2 = 6.0
DEPTH (M)
0
20
40
60
80
100
0
10
20
30
40
50
60
70
80
90
ANGLE OF INCIDENCE θ°

Figure 19

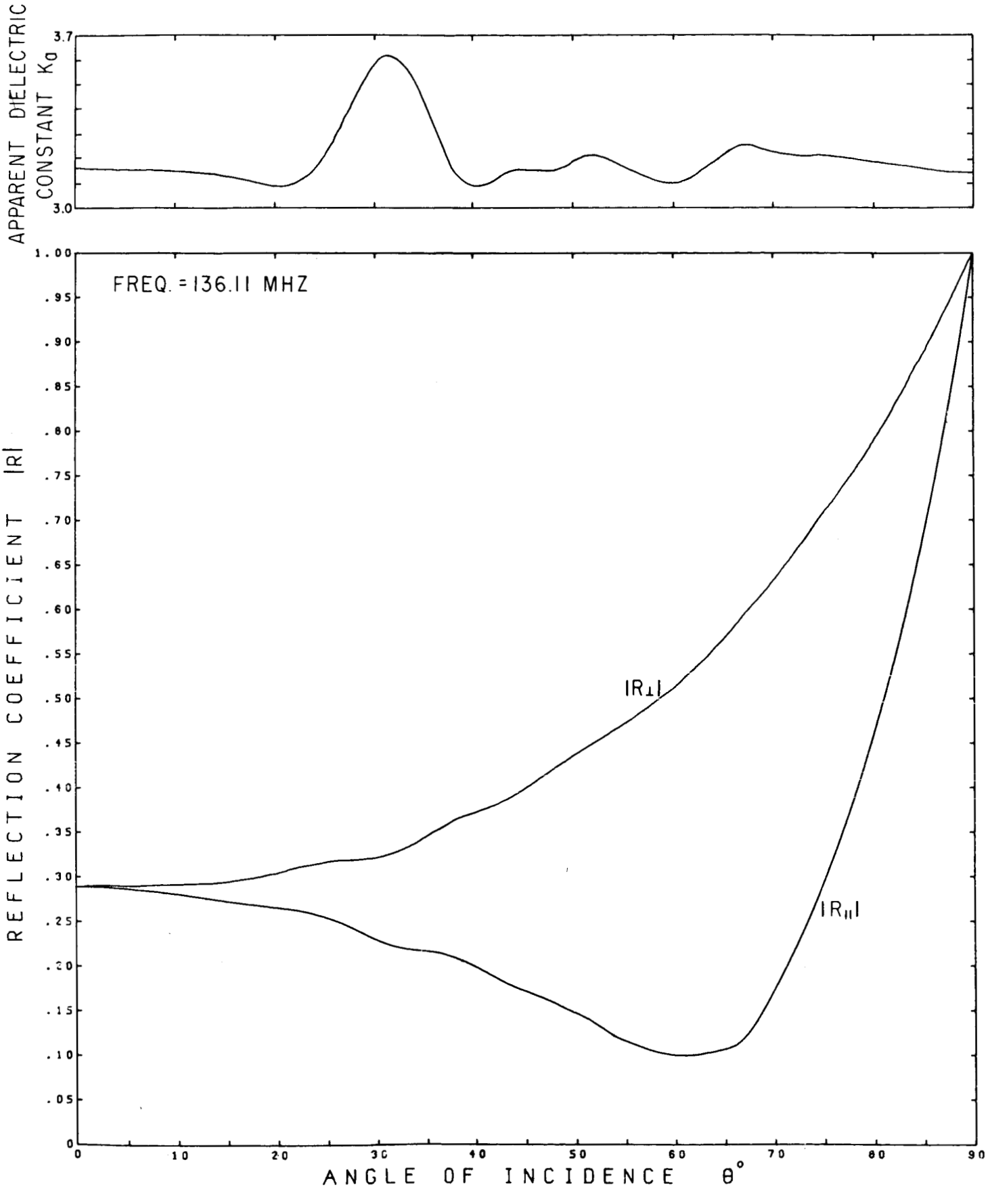
APPARENT DIELECTRIC CONSTANT K_a
3.7
3.0
FREQ. = 136.11 MHZ
REFLECTION COEFFICIENT |R|
1.00
.95
.90
.85
.80
.75
.70
.65
.60
.55
.50
.45
.40
.35
.30
.25
.20
.15
.10
.05
0
$|R_\perp|$
$|R_{||}|$
0
10
20
30
40
50
60
70
80
90
ANGLE OF INCIDENCE θ°

Figure 20